Chapter 21B. Analysis of Imaging Spectrometer Data for the Khanneshin Area of Interest

By Raymond F. Kokaly and Michaela R. Johnson

Abstract

Imaging spectrometer data collected over the Khanneshin area of interest (AOI) in southwestern Afghanistan were analyzed with spectroscopic methods to identify the occurrence of selected materials at the surface. HyMap imaging spectrometer data collected in 2007 covers the northeastern two-thirds of the Khanneshin AOI. Absorption features in the spectra of HyMap data were compared to a reference library of spectra of known materials. The illite and muscovite classes cover most of the eastern portion of the Khanneshin AOI. The carbonate mixed with clay class is widely distributed throughout the area, but is most concentrated in the northern and western portions of the AOI. Pixels matched to iron-bearing carbonate, calcite, dolomite, and mixtures of dolomite with montmorillonite and/or calcite are concentrated in the mapped intrusive rock unit of the volcano and adjacent areas. The central carbonatite volcanic area, containing the Khanneshin rare-earth-elements (REE) occurrence is defined by calcite in the 2-micrometer (μm) map and the lack of iron-bearing minerals in the 1-μm map. The distribution pattern of pixels with this composition includes the central vent of the Khān Nishīn Ghar volcano and mapped intrusive rocks, as well as a larger area of carbonatite stretching north and east from the mapped intrusive body. In addition, a great deal of mineral variation around the main areas of carbonatite was detected in the 2-μm map, which included occurrences of dolomite, calcite+dolomite or serpentine, montmorillonite, and iron-bearing carbonate; and in the 1-μm map, which included various types of ferric and ferrous iron-absorption features. In conjunction with the carbonate absorption feature, the variations in iron absorption may be related to the concentration of REE and uranium in the Khanneshin AOI. Pixels identified as containing iron-bearing carbonate within the more widespread calcite+montmorillonite class are concentrated near the southern margin of the volcano in the area around the Khanneshin southern uranium occurrence. This pattern of materials match the mineral occurrence description of sandstone intruded by carbonatite dikes along southwest-striking faults, with the fault zones containing ferruginous clay carbonate minerals. If the uranium-bearing sandstones are associated with the fault zones indicated by iron-bearing carbonate, then the distribution of this mineral identified in the imaging spectrometer data indicates a large area stretching from the known mineral occurrence, Khanneshin southern, to the northwest, covering a distance of more than 11 kilometers. An area north of the volcano, which includes Khanneshin northern uranium-thorium mineral occurrence, contains scattered pixels matched to montmorillonite clay within the more widely mapped calcite+montmorillonite class. This pattern corresponds with the description of the host rock for the uranium occurrence. Further analyses of the HyMap imaging spectrometer data are warranted, including spectral measurements of REE-containing samples from the Khanneshin AOI. The HyMap imaging spectrometer data may be able to directly detect the signatures of rare-earth-minerals (REM) if they occur in great enough abundance within a pixel.

21B.1 Introduction

Past studies of geologic data from Afghanistan revealed numerous areas with indications of potential mineral resources of various types (Peters and others, 2007; Abdullah and others, 1977). Several of these areas were selected for follow-on studies using imaging spectroscopy to characterize surface materials; imaging spectroscopy is an advanced type of remote sensing, also known as

hyperspectral remote sensing. One of the areas with potential mineral resources is the Khanneshin area of interest (AOI) in southwestern Afghanistan, which is approximately 690 kilometers (km) southwest of Kabul (fig. 21B–1). The area is believed to have the potential for rare earth elements (REE), uranium, and thorium. To help assess these potential resources, high-resolution imaging spectrometer data, covering most of the Khanneshin AOI, were analyzed to detect the presence of selected minerals that may be indicative of past mineralization processes. This report contains the results of the spectroscopic data analyses and identifies sites within the Khanneshin AOI that deserve further investigation, especially detailed geological mapping, lithologic sampling, and geochemical studies.

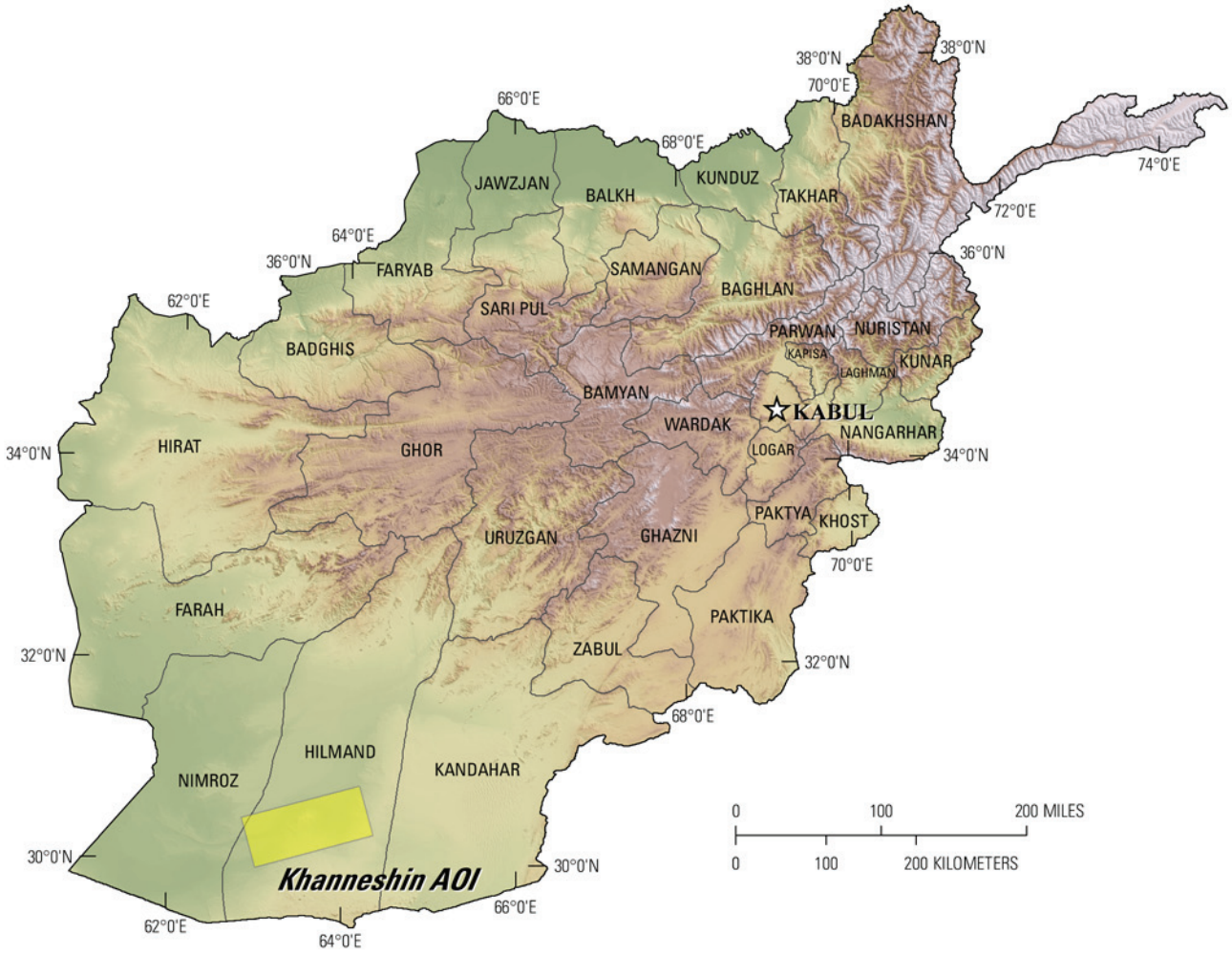

Figure 21B–1. Index map of the Khanneshin area of interest, southwestern Afghanistan.

21B.2 Data Collection and Processing

In 2007, imaging spectrometer data were acquired over most of Afghanistan as part of the U.S. Geological Survey (USGS) project "Oil and Gas Resources Assessment of the Katawaz and Helmand Basins." These data were collected to characterize surface materials in support of assessments of resources (coal, water, minerals, oil, and gas) and earthquake hazards in the country (King and others, 2010). Imaging spectrometers measure the reflectance of visible and near-infrared light from the Earth's surface in many narrow channels, producing a reflectance spectrum for each image pixel. These reflectance spectra can be interpreted to identify absorption features that arise from specific chemical transitions and molecular bonds that provide compositional information about surface materials. Imaging spectrometer data can only be used to characterize exposed surface materials, not subsurface composition or structure. Subsurface processes can be indicated, however, by the distribution of surface

materials. The HyMap imaging spectrometer data, collected in 2007, cover the northeastern two-thirds of the Khanneshin AOI.

21B.2.1 Collection of Imaging Spectrometer Data

The HyMap imaging spectrometer (Cocks and others, 1998) was flown over Afghanistan from August 22 to October 2, 2007 (Kokaly and others, 2008). HyMap has 512 cross-track pixels and covers the wavelength range from 0.43 to 2.48 microns (μm) in 128 channels. The imaging spectrometer was flown on a WB-57 high-altitude aircraft at approximately 50,000 feet. There were 207 standard data flight lines and 11 cross-cutting calibration lines collected over Afghanistan for a total of 218 flight lines, covering a surface area of 438,012 square kilometers (km^2) (Kokaly and others, 2008). Data were received in scaled radiance (calibrated to National Institute of Standards and Technology reference materials). Before processing, four channels that had low signal-to-noise and (or) were in wavelength regions that overlapped between detectors were removed from the image cubes. Each flight line was georeferenced to Landsat Thematic Mapper (TM) base imagery in Universal Transverse Mercator (UTM) projection (Davis, 2007).

21B.2.2 Calibration Procedure

HyMap data were converted from radiance to reflectance using a multi-step process. This calibration process removed the influence of the solar irradiance function, atmospheric absorptions and residual instrument artifacts, resulting in reflectance spectra that have spectral features that arise from the material composition of the surface. Because of the extreme topographic relief and restricted access to ground calibration sites, modifications to the standard USGS calibration procedures were required to calibrate the 2007 Afghanistan HyMap dataset (Hoefen and others, 2010). In the first step of the calibration process, the radiance data were converted to apparent surface reflectance using the radiative transfer correction program Atmospheric CORrection Now (ACORN; ImSpec LLC, Palmdale, Calif.). The ACORN program was run multiple times for each flight line, using average elevations in 100-meter (m) increments, covering the entire elevation range along the flight line. A single atmospherically corrected image was assembled from these elevation-incremented ACORN results. This was done by determining the elevation of each HyMap pixel and selecting the atmospherically corrected pixel from the 100-meter increment closest to that elevation.

Each assembled atmospherically corrected image was further empirically adjusted using ground-based reflectance measurements from a ground calibration site. Spectra for five ground calibration sites were collected in Afghanistan; specifically, the field spectra of ground targets at Kandahar Air Field, Bagram Air Base, and Mazar-e-Sharif Airport, and laboratory spectra of soil samples collected from two fallow fields in Kabul. These spectra were used to calculate empirical correction factors using the pixels of atmospherically corrected HyMap data from the flight lines that passed over the sites. The empirical correction from the closest calibration site to each flight line was then applied.

To further improve the data quality, an additional calibration step was taken to address the atmospheric differences caused, in part, by the large distances between the calibration sites and the HyMap survey area. The large distances were the result of a lack of safe access to ground calibration sites. The duration of the airborne survey and variation in time of day during which flight lines were acquired also resulted in differences in atmospheric conditions between standard flight lines and lines over ground calibration sites. Thus, over the course of the data collection, the sun angle, atmospheric water vapor, and atmospheric scattering differed along and between flight lines. To compensate for this variation, cross-cutting calibration flight lines over the ground calibration areas were acquired (Kokaly and others, 2008) and used to refine the data quality of standard data lines. A multiplier correction for each standard data line, typically oriented north-south, was derived using the pixels of overlap with the well-calibrated cross-cutting line that intersected it, subject to slope, vegetation cover, and other

restrictions on pixel selection (Hoefen and others, 2010). As a result, the localized cross-calibration multiplier, derived from the region of overlap, corrected residual atmospheric contamination in the imaging spectrometer data that may have been present after the ground-calibration step.

21B.2.3 Materials Maps and Presentation

After undergoing the calibration process, the reflectance data were georeferenced and then analyzed using the Material Identification and Characterization Algorithm (MICA), a module of the USGS Processing Routines in Interactive Data Language (IDL) for Spectroscopic Measurements (PRISM) software (Kokaly, 2011). The MICA analysis compared the reflectance spectrum of each pixel of HyMap data to entries in a reference spectral library of minerals, vegetation, water, and other materials. The HyMap data were compared to 97 reference spectra of well-characterized mineral and material standards. The best spectral match to each pixel was then determined and the results were clustered into classes of materials discussed next. The resulting maps of material distribution, resampled to a 23 × 23-m square pixel grid, were mosaicked to create thematic maps of surface mineral occurrences over the full data set covering Afghanistan.

The MICA module was applied to HyMap data twice in order to present the distribution of two categories of minerals naturally separated in the wavelength regions of their primary absorption features. MICA was applied using the subset of minerals with absorption features in (1) the visible and near-infrared wavelength region to produce the 1-µm map of iron-bearing minerals and other materials (King and others, 2011), and (2) the shortwave infrared region to produce the 2-µm map of carbonates, phyllosilicates, sulfates, altered minerals, and other materials (Kokaly and others, 2011). For clarity of presentation, some individual classes in these two maps were bundled by combining selected mineral types (for example, all montmorillonites or all kaolinites) and representing them with the same color in order to reduce the number of colors required to represent the mineral classes.

The iron-bearing mineral results were grouped into 28 classes. Iron-bearing minerals with different mineral compositions but similar broad spectral features are difficult to classify as specific mineral species. Thus, generic spectral classes, including several minerals with similar absorption features, such as Fe^{3+} Type 1 and Fe^{3+} Type 2, are depicted on the map. The carbonates, phyllosilicates, sulfates, and altered minerals map was categorized into 32 classes. Minerals with slightly different chemical compositions but comparable spectral features are less easily distiguished; therefore, some identified classes consist of several minerals with similar spectra, such as the "chlorite or epidote" class. When comparisons with reference spectra resulted in no viable match, a designation of "not classified" was assigned to the pixel.

21B.3 Geologic Setting of the Khanneshin Area of Interest

The Khanneshin AOI is mostly within the Hilmand Province in southwestern Afghanistan except for the northeastern corner, which is in the Nimroz Province. The contrast-enhanced stretch of the natural color composite of Landsat Thematic Mapper bands in figure 21B–2 provides a general overview of the Khanneshin AOI terrain and is useful for understanding the general characteristics and distribution of surficial material, including rocks and soil, unconsolidated sediments, vegetation, and hydrologic features.

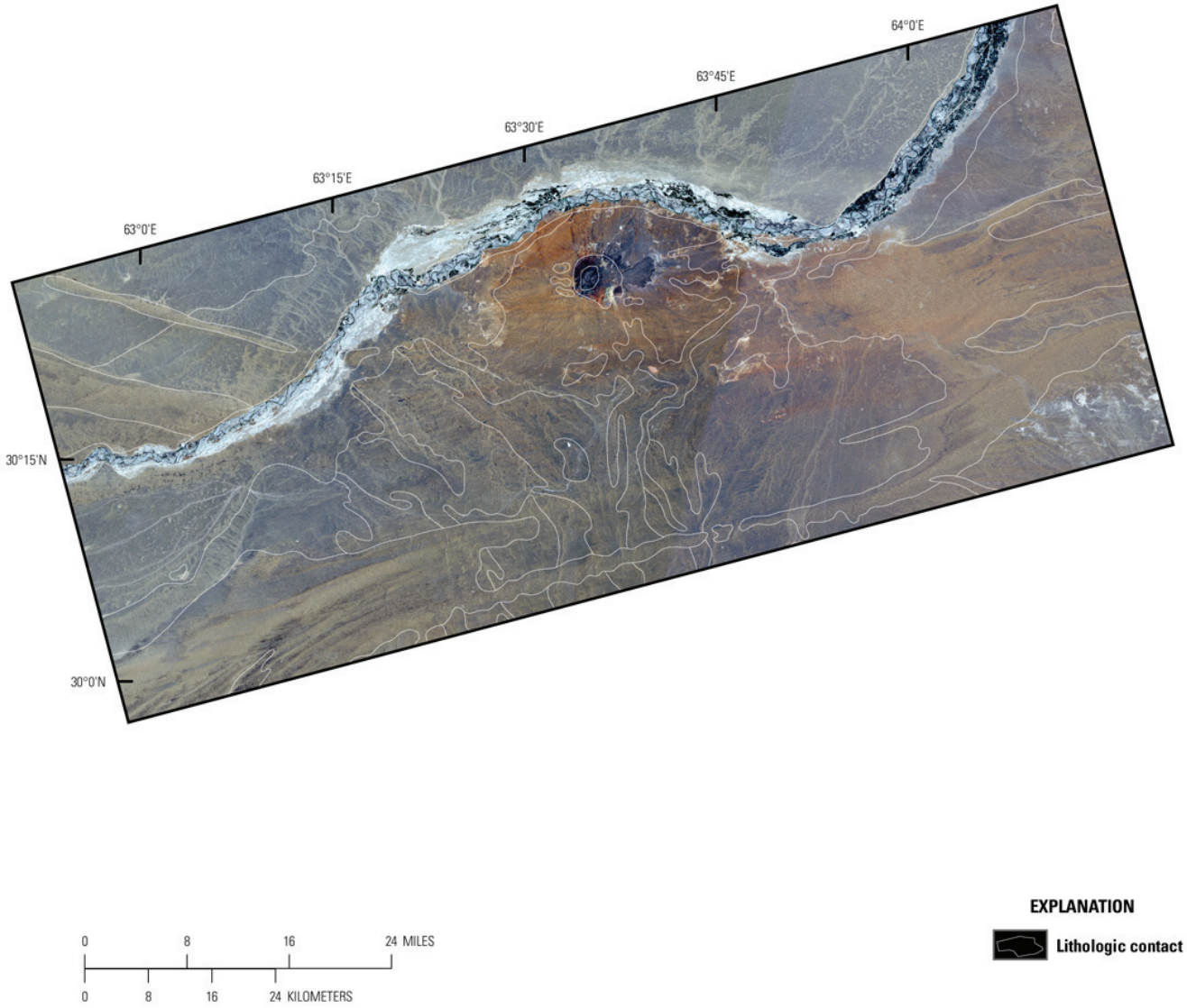

Figure 21B–2. Contrast-enhanced Landsat Thematic Mapper natural-color image of the Khanneshin area of interest. Contacts are from Abdullah and Chmyriov (1977).

21B.3.1 Topography

Elevations in the Khanneshin AOI range between 559 and 1,287 m (fig. 21B–3). The highest areas are the Khān Nishīn Ghar volcano in the center of the Khanneshin AOI, and along the southern edge of the area. The low areas include the Hilmand River and adjacent agricultural areas in the northern portion of the AOI.

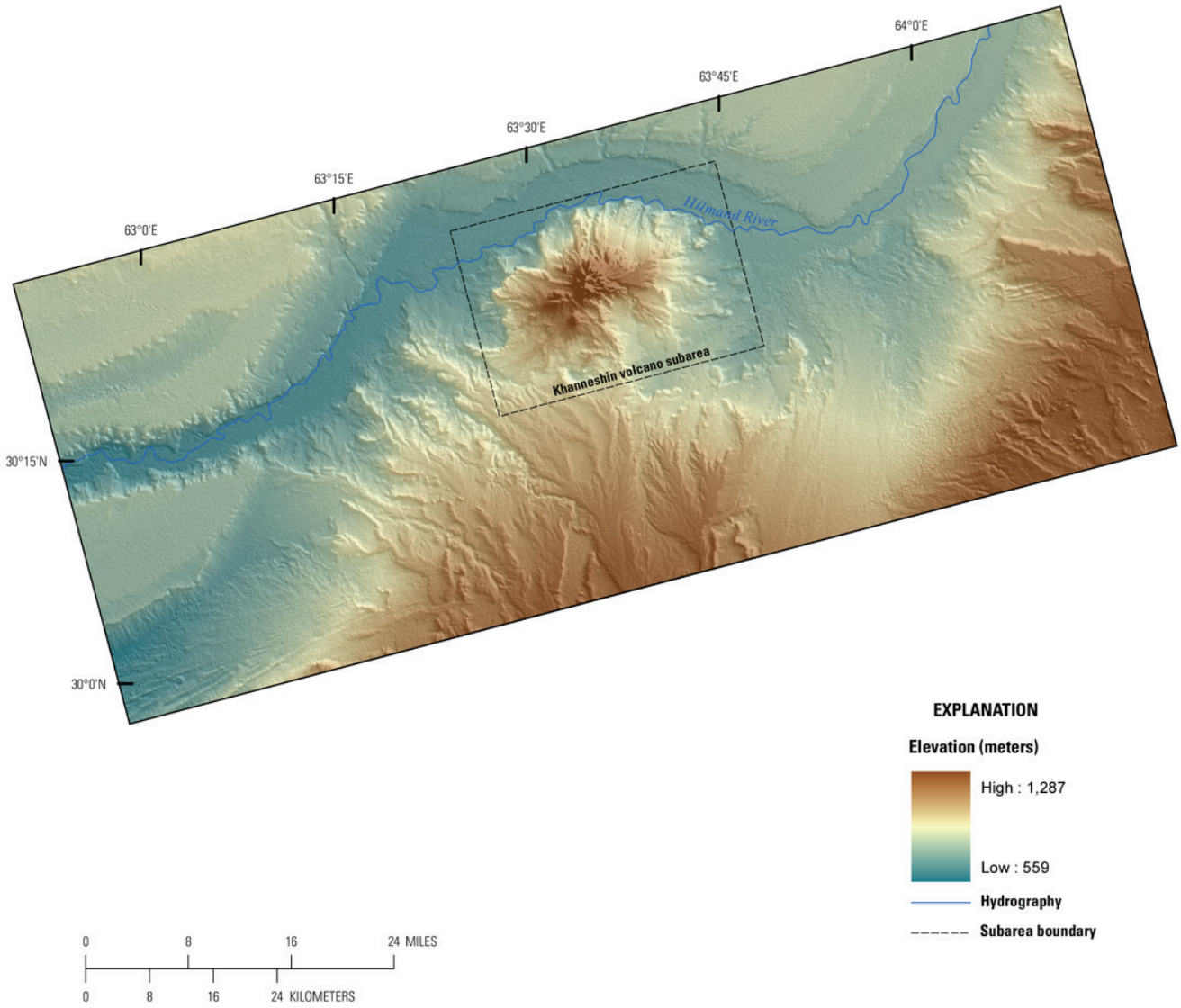

Figure 21B–3. Elevations and topography in the Khanneshin area of interest.

21B.3.2 Lithology and Structure

Carbonatite and syenite intrusive rocks have been identified in southern Afghanistan as small volcanoes, plugs, and dikes in the Helmand Basin in the southern part of the country (Abdullah and others, 1975; Vikhter and others, 1975, 1976, 1978). Carbonatites may produce large deposits of REE, copper, phosphate, vermiculite, and other commodities, and therefore, identification and documentation of their location, size, and character is important (Alkhazov and others, 1977, 1978). The oldest rocks in the Khanneshin AOI are Late Pliocene stratified rocks described as including gray conglomerate, gravelstone, sandstone, siltstone, clay, limestone, marl, gypsum, salt, and acidic and mafic volcanic rocks (fig. 21B–4; Abdullah and Chmyriov, 1977; Doebrich and others, 2006). Quaternary and Recent rocks, including shingly and detrital sediments, gravel, sand, clay, clay sand, loam, loess, cover most of the Khanneshin AOI.

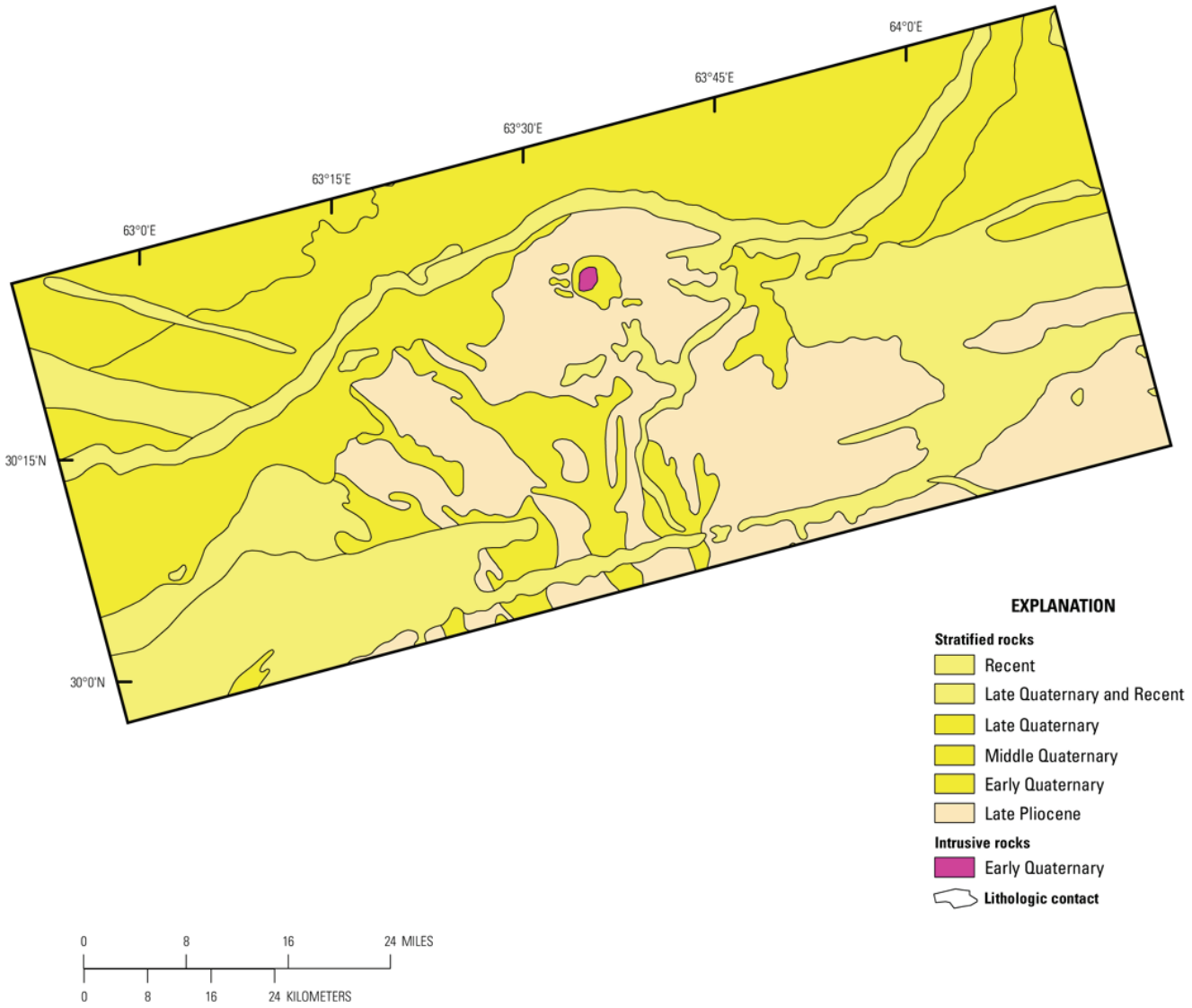

Figure 21B–4. Geologic map of the Khanneshin area of interest from digital geologic map of Afghanistan (Doebrich and others, 2006; Abdullah and Chmyriov, 1977).

As noted earlier, the Khanneshin AOI includes a volcanic cone (map units Q1kt and Qtcab, of Doebrich and others, 2006). In addition, the AOI includes north-striking carbonatite dikes to the east and west of the volcanic cone that roughly follow the shape of aeromagnetic anomalies beneath cover (Peters and others, 2007). A subarea was delineated to encompass the central volcanic area, the three mineral occurrences, and the local shape of the aeromagnetic signature; the subarea is referred to as the Khanneshin volcano subarea. The uranium-thorium mineralization in the subarea is distributed over a 40 km^2 area and includes tuff, agglomerate, and subvolcanic carbonatitic igneous rocks. The main carbonatite rock types are soevite, barite-ankerite-fluorite carbonatite and associated tuff, alvikite and associated agglomerate and tuff, as well as leucite phonolite. The rocks have high concentrations of REE, uranium, strontium, fluorite, phosphorous, niobium, and lead. The REE concentrations are highest in the soevitic rocks and in ankerite-barite carbonatite. The ankerite-barite carbonatite contains REE barium-strontium carbonate minerals associated with fluorite. In some fluorite zones, REE concentrations are several percent, accompanied by high concentrations of barite (up to 15 percent).

21B.3.3 Known Mineralization

REE and uranium-bearing minerals were discovered in 1974 at the Khanneshin volcano, and the zones are documented in geologic maps, aerial radiometric surveys, topographic grids, and trench sampling results. The reports show REE and uranium occurrences over much of the volcanic cone. Most samples from REE occurrences yield average total REE percentages between 1.5 and 3 percent, but the vertical orientation of the occurrences hinders the estimation of REE tonnage. Figure 21B–5 shows three locations where mineralization with a potential for mineral resource development may exist (Peters and others, 2007). A number of different types of mineral occurrences, particularly REE, uranium, and thorium, are present within the Khanneshin AOI. The mineralogical characteristics of the mineralized locations are summarized in table 21B–1.

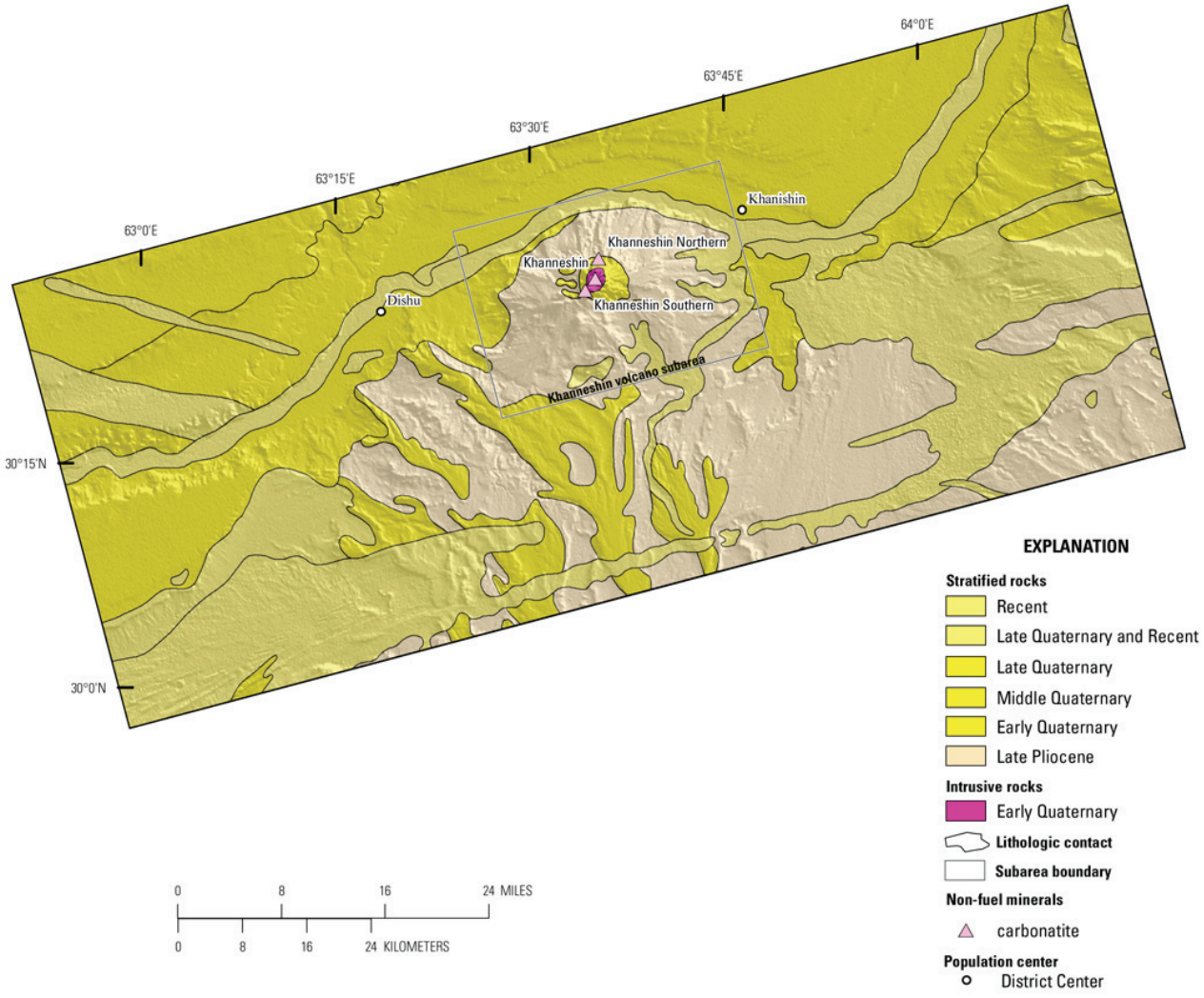

Figure 21B–5. Sites of known mineralization by deposit type (Peters and others, 2007) on the geologic map of the Khanneshin area of interest from 1:500,000-scale geologic map of Afghanistan (from Doebrich and others, 2006; Abdullah and Chmyriov, 1977).

Table 21B–1. Sites of known sites of mineralization in the Khanneshin area of interest (Peters and others, 2007).
[REE, rare earth element; U, uranium; m, meter; km, kilometer]

Name	Deposit type	Major commodity	Deposit size, description	Alteration	Mineralogy	Gangue
Khanneshin	Carbonatite	REE, U	Occurrence	Calcite alteration; barite-ankerite-fluorite alteration	No data	Calcite; fluorite; ankerite; barite
Khanneshin Southern	Carbonatite	U	Occurrence, thickness: 0.5 m with extent 0.3 to 1.5 km; extent: more than 300 m; thickness: 14.2_58 m; depth: 100 m; weathering zone thickness: up to 5 m	Dolomitization; chloritization; calcite alteration; barite-ankerite-calcite alteration	Hydronasturan; autunite; torbernite; uranite; pyrochlore; monazite; thorbastnaesite	Dolomite; chlorite; calcite; barite; ankerite
Khanneshin Northern	Carbonatite	U	Occurrence, width up to 25 m with extent up to 2 km	Silicification	No data	Quartz

The southern Khanneshin uranium occurrence near the southern margin of the Khān Nishīn Ghar volcano is 300 to 1,500 m long and up to 0.5 m wide and contains uranium-bearing Neogene sandstone intruded by carbonatite dikes along southwest-striking faults that intersect radial fractures and carbonatite dikes. The fault zones contain ferruginous clay carbonate minerals as cement in the hydrothermally altered sandstone, which is replaced by dolomite and chlorite. The southern uranium area also contains four mineralized zones, one of which is over 300 m long and 14.2 to 58.0 m wide, and is exposed by erosion to a 100-m depth. The most porous zones of coarse-grained sandstone contain the greatest uranium concentrations along strong fractures and joints. The 2-millimeter (mm) to 1.3-centimeter (cm)-wide uranium-bearing veinlets are symmetrically banded with outer dolomite selvages grading 0.5 percent cerium, 0.4 percent lanthanum, and 0.2 percent barium. The inner parts of the veinlets consist of calcite with barium minerals. In the wide parts of the veinlets, hyalite and uranium-bearing aragonite are present. The oxidized zone is up to 5.0 m wide and contains uranium silicate minerals, hydrous and phosphatic uranium minerals, and uranium-bearing gypsum (Abdullah and others, 1977).

The northern uranium-thorium Khanneshin mineral occurrence is hosted in sandy claystone in a 2,000-m-long and up to 25-m-wide silicified zone grading 0.006 to 0.015 percent uranium and 0.002 to 0.010 percent thorium (Abdullah and others, 1977).

The vent of the Khān Nishīn Ghar volcano is composed of ankerite-barite carbonatite associated with an 800-m-long, 50-m-wide fluorite-rich zone that is eroded to a 150-m depth and contains abundant earthy-yellow strontium-barium zones grading 0.3 to 2.0 and up to 6.0 percent REE, more than 10 percent strontium, and 10 percent barium. Fluorite in the complex also contains REE, grading 0.6 percent cesium, 0.5 percent lanthanum, and 0.05 percent uranium.

21B.4 Mineral Maps of the Khanneshin Area of Interest

Analysis of the HyMap imaging spectrometer data of the Khanneshin AOI using spectroscopic methods resulted in the identification of a wide variety of minerals exposed at the surface. Although the occurrence of certain minerals may suggest that mineralization processes may have once operated in the area, many of the minerals that were identified are also common rock-forming minerals or minerals that can be derived from the weathering of a wide variety of rock types. Consequently, the distribution patterns of the identified minerals and the geologic context in which they occur are essential to understanding the causes of mapped mineral occurrences and evaluating the possible potential for related mineral deposits.

Figures 21B–6 depicts the results of the MICA analyses of the HyMap data for the Khanneshin AOI for the 2-µm materials, which include clays, carbonates, phyllosilicates, sulfates, altered minerals and other materials. Figure 21B–7 shows the results for the iron-bearing minerals. The illite and

muscovite classes cover most of the eastern portion of the Khanneshin AOI. The calcite mixed with clay class is also distributed widely throughout the area, but is most concentrated in the northern and western portions of the AOI. Pixels matched to iron-bearing carbonate, calcite, dolomite, and mixtures of dolomite with montmorillonite and (or) calcite are concentrated in the mapped intrusive rock unit of the Khān Nishīn Ghar volcano and adjacent areas. Distinct patterns of montmorillonite and kaolinite clays, calcite, and gypsum occur in localized concentrations sporadically throughout the central and eastern portions of the AOI. The Fe^{3+} Type 1 class is distributed in a similar pattern as the muscovite/illite classes (see fig. 21B–6), covering the majority of the eastern portion of the Khanneshin AOI. Pixels matching the Fe-hydroxide class are mapped in contiguous patterns in this part of the AOI and surrounding the mapped units of volcanic rocks. In the area of the Khān Nishīn Ghar volcano, iron-bearing minerals were not detected (see black pixels of "not classified" category, fig. 21B–6); in fact, this category corresponds well with the calcite class of the 2-µm map. Immediately surrounding the intrusive body, large areas of hematite and smaller concentrations of goethite, Fe^{2+} Fe^{3+} Types 1 and 2, and Fe^{3+} Type 1, are present in patterns distinctly different from those in the rest of the Khanneshin AOI.

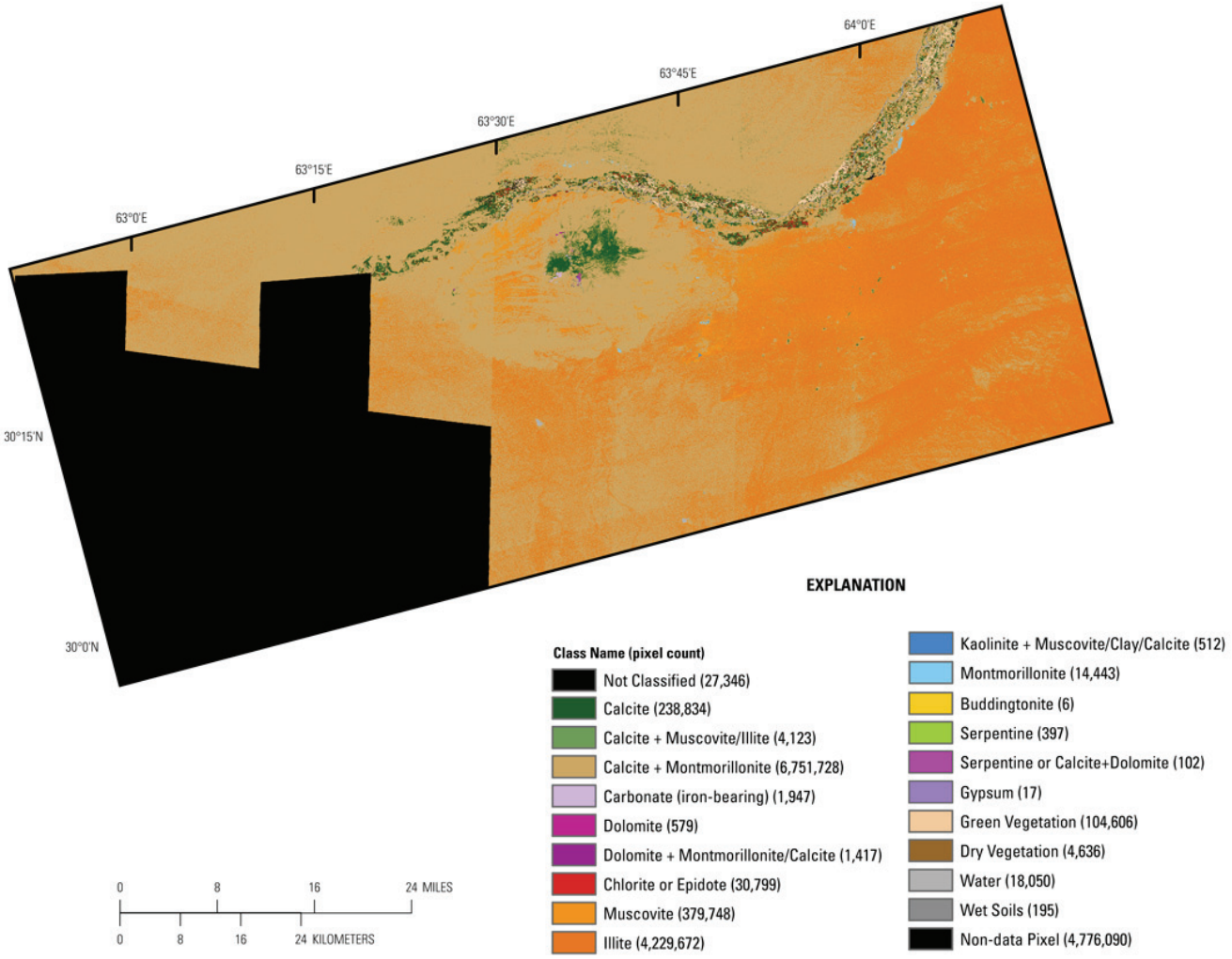

Figure 21B–6. Map of carbonates, phyllosilicates, sulfates, altered minerals, and other materials derived from HyMap data in the Khanneshin area of interest.

Because of the large number of classes represented and the subtleties of the represented distribution patterns, it is instructive to display these results as a series of image maps, each depicting a selected group of minerals that are mineralogically related or commonly occur together in specific geologic environments (figs. 21B–8 through 21B–12). Figure 21B–8 shows the distribution of carbonate

minerals in the Khanneshin AOI, whereas figure 21B–9 shows the distribution of clay minerals and micas. The distributions of iron oxide and hydroxide minerals are shown in figure 21B–10. Minerals commonly found in hydrothermally altered rocks are shown in figure 21B–11 and secondary minerals often associated with mineralized and/or weathered rocks are shown in figure 21B–12. Maps focused on the Khān Nishīn Ghar volcano (portrayed herein as the Khanneshin volcano subarea), are presented following the maps and discussion of the entire Khanneshin AOI.

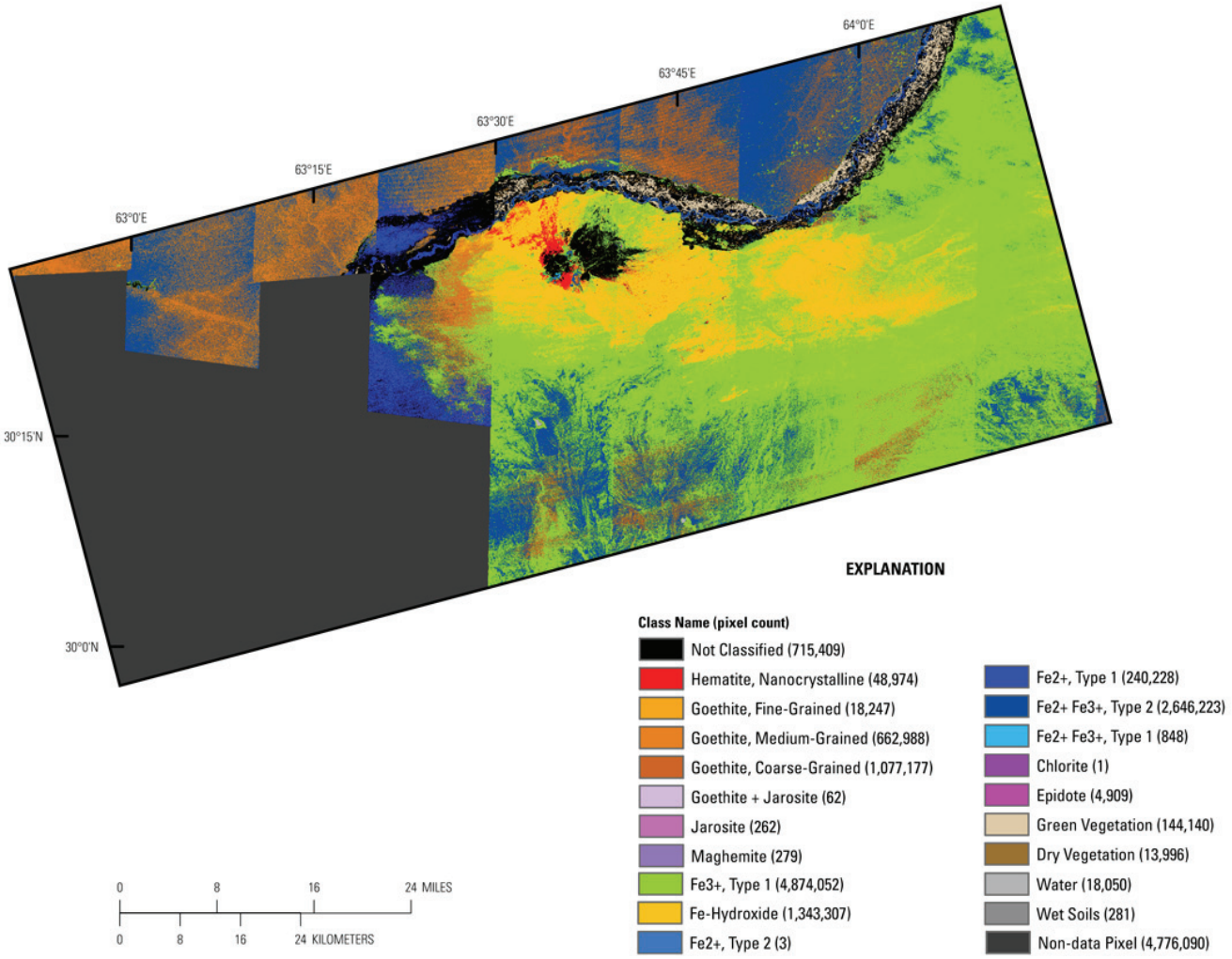

Figure 21B–7. Map of iron-bearing minerals and other materials derived from HyMap data in the Khanneshin area of interest.

21B.4.1 Carbonate Minerals

The calcite mixed with clay class is distributed widely throughout the AOI, but is most contiguous in the northern and western portions of the AOI (fig. 21B–8). Pixels matched to iron-bearing carbonate, calcite, dolomite, and mixtures of dolomite with montmorillonite and/or calcite are concentrated in the mapped intrusive rock unit of the Khān Nishīn Ghar volcano and adjacent areas. Calcite also occurs along the Hilmand River, potentially in areas of evaporation that produce a caliche layer at the surface.

21B.4.2 Clays and Micas

Illite was detected abundantly in the Khanneshin AOI (fig. 21B–9), often in a diffuse pattern. Local-scale concentrations of montmorillonite were mapped, especially along the Helmand River;

extents ranged from hundreds of meters up to a few kilometers. A few concentrations of kaolinite mixed with carbonate and (or) other clays were also detected in the HyMap data. The montmorillonite (lat 30°22'08"N., long 63°40'32"E., and lat 30°24'16" N., long 63°47'53" E.) and kaolinite (lat 30°21'54" N., long 63°47'16" E.) occurrences in some areas may indicate ephemeral ponds and small lakes. Small lakes with standing water were detected in the Khanneshin AOI (lat 30°16'49" N., long 63°34'04" E., and lat 30°10'03" N., long 63°46'13" E.; fig. 21B–6).

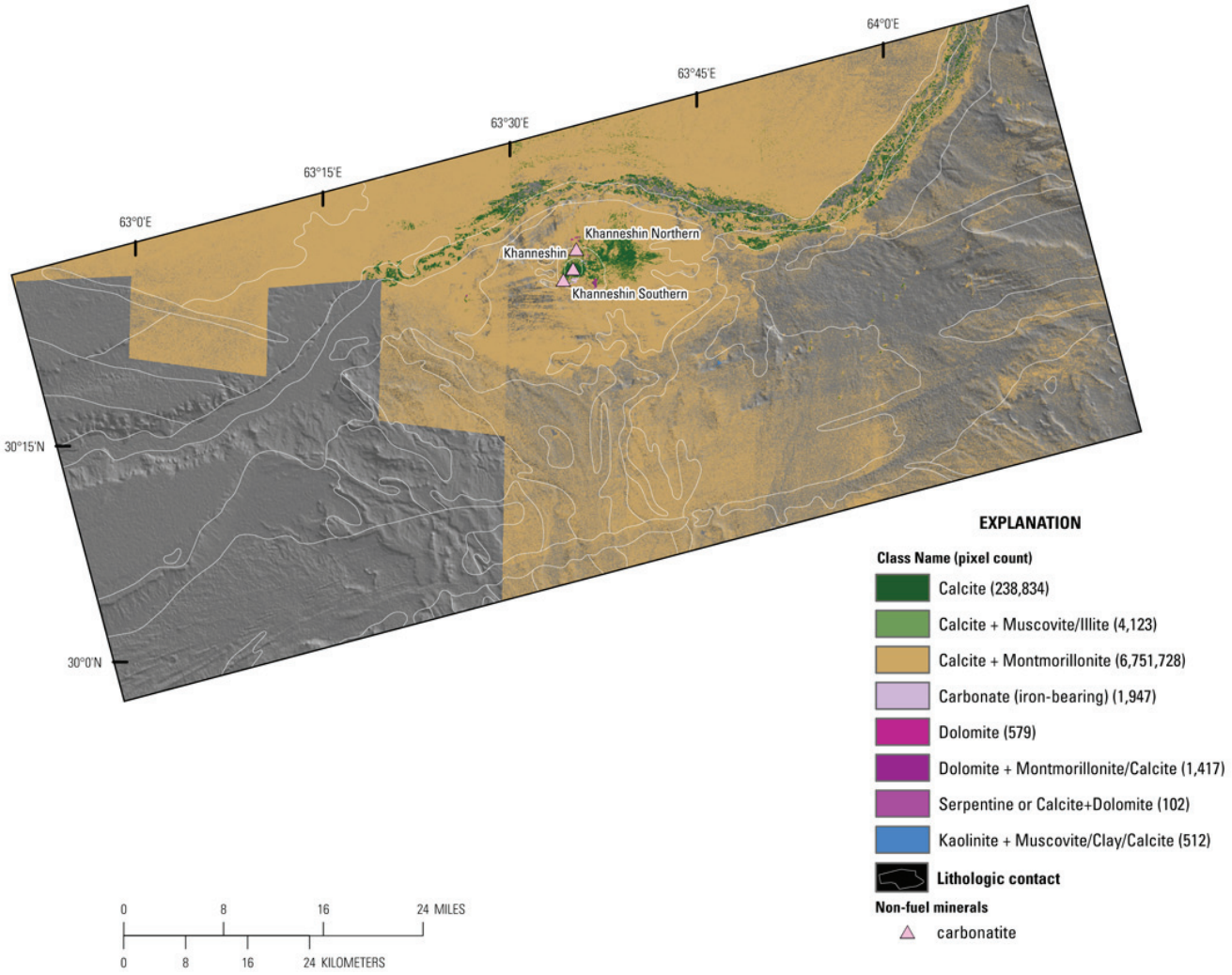

Figure 21B–8. Map of distribution of carbonate minerals derived from HyMap data in the Khanneshin area of interest.

21B.4.3 Iron Oxides and Hydroxides

The Khanneshin AOI contains a large area of Fe-hydroxide on the lower slopes of the intrusive body in the central part of the area (fig. 21B–10). This material was also detected to the east of the Khān Nishīn Ghar volcano, in a pattern that appears to be the result of redistribution of the material by wind. At higher elevations, closer to the center of the volcano, patterns of hematite and goethite were detected at the edge of the intrusive rock unit in which calcite was mapped (figs. 21B–6 and 21B–10). The iron oxides and hydroxides, as well as the iron-bearing carbonate (fig. 21B–6) and ferric iron mineral groups, Fe^{2+} Fe^{3+} Types 1 and 2 and Fe^{3+} Type 1 (fig. 21B–7), described previously, occur within the Early Quaternary stratified rock unit, and are likely useful for differentiating tuffs and lavas within the Khanneshin group. This pattern of a central calcite body with surrounding areas of iron-bearing minerals

extends beyond the mapped intrusive and stratified rock unit of the volcano to an adjacent area to the east, covering approximately 4,000 hectares.

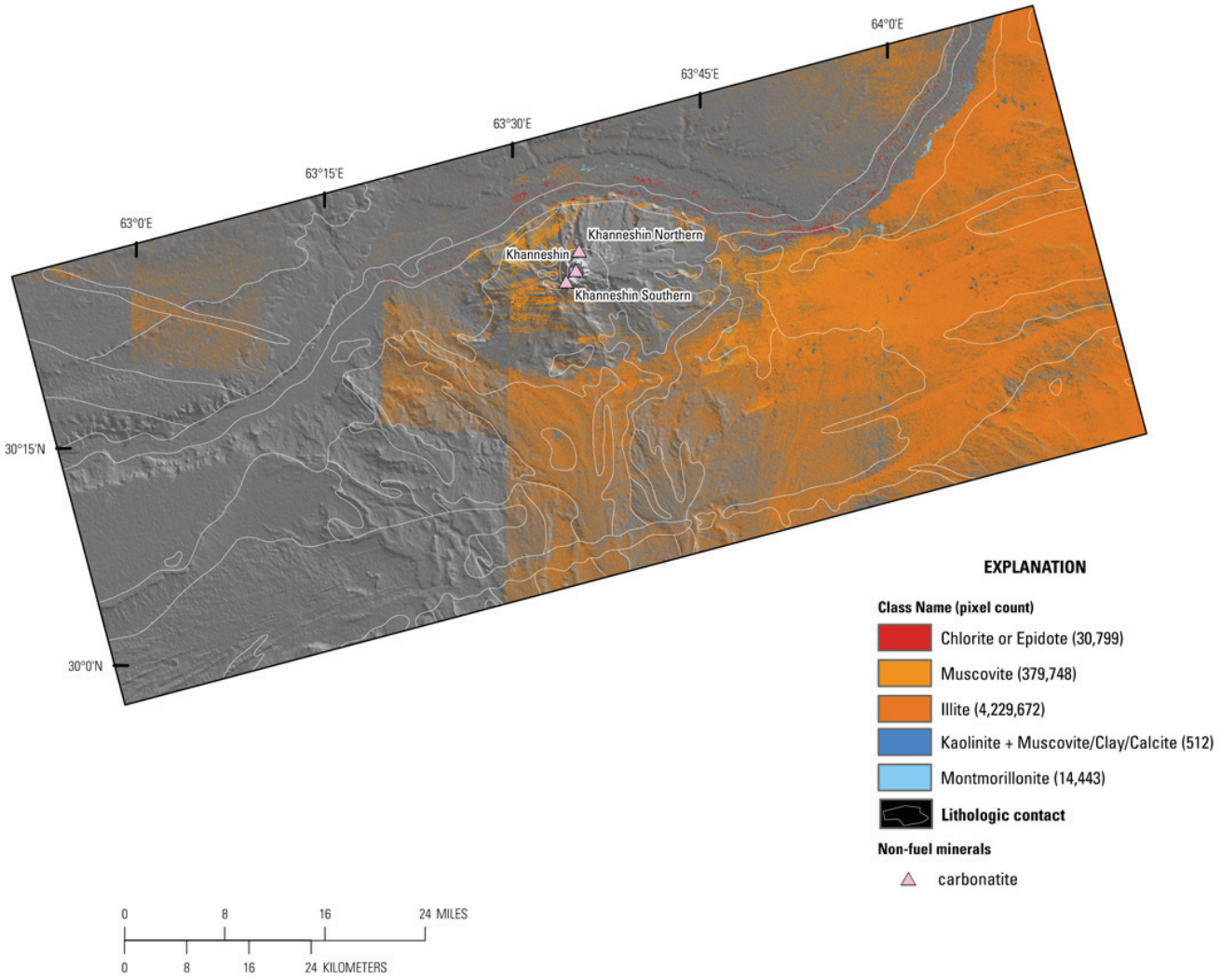

Figure 21B–9. Map of distribution of clay and mica minerals derived from HyMap data in the Khanneshin area of interest.

21B.4.4 Common Alteration Minerals

Most of the minerals in this group are commonly present in hydrothermally altered rocks associated with epithermal mineral deposits (fig. 21B–11). Consequently, the locations of distinct clusters are of great interest in terms of potential mineral deposits. However, the mineral identifications and distributions are not suggestive of such alteration in the Khanneshin AOI. The map shows the distribution of the iron-bearing carbonate class along a southwest-to-northeast trend, most heavily concentrated along the southern contact of the mapped intrusive rocks.

Common Secondary Minerals

Secondary minerals, in the chlorite or epidote class (fig. 21B–12) occur mostly along the Helmand River in the Khanneshin AOI. Inspection of the spectra from this area indicates they contain a dry vegetation feature at 2.1 μm in addition to the 2.3-μm feature expected for these minerals;these spectral features indicate the chlorite or epidote pixels are actually areas of calcite, which has a 2.3-μm

feature, covered by some dry vegetation, which imparts the 2.1-µm feature. Scattered pixels of the serpentine and "serpentine or calcite + dolomite" classes were detected in the intrusive rock unit, and are likely indicating calcite+dolomite because they are mapped on the edges of areas identified as containing dolomite (fig. 21B–6).

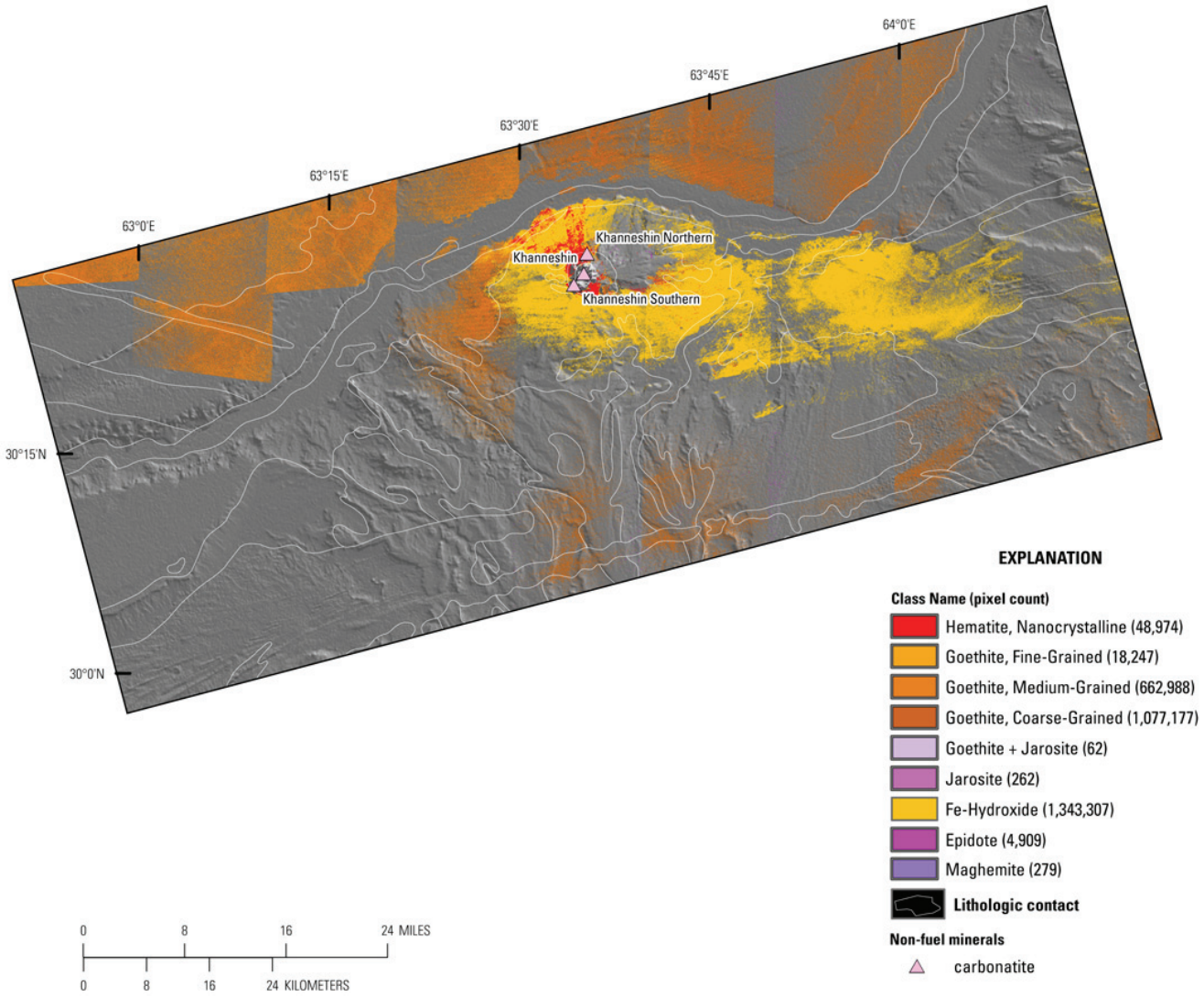

Figure 21B–10. Map of distribution of iron oxide and hydroxide derived from HyMap data in the Khanneshin area of interest.

21B.4.5 Khanneshin Volcano Subarea

Maps of the subarea around the Khān Nishīn Ghar volcano are shown in increased detail in figures 21B–13 through 21B–19, which portray the maps of Landsat TM imagery, geology with known mineral occurrences, 2-µm materials, 1-µm materials, carbonate, Fe-oxide and hydroxide, and common alteration minerals.

Figure 21B–13 shows the Khanneshin southern mineral occurrence at the boundary separating the darker volcanic rocks and the lighter, red area in the stratified rock unit surrounding the volcano (fig. 21B–14). The mineral maps derived from the imaging spectrometer data show the rocks in the vicinity of this mineral occurrence to be mapped in the calcite+montmorillonite clay and iron-bearing carbonate classes in the 2-µm map (fig. 21B–15), with the iron absorption feature identified generally as a ferric iron mineral (Fe^{3+} type 1; fig. 21B–16). The setting of the southern Khanneshin uranium

occurrence is described as being near the southern margin of the volcano in uranium-bearing Neogene sandstone intruded by carbonatite dikes along southwest-striking faults, with the fault zones containing ferruginous clay carbonate minerals as cement in the hydrothermally altered sandstone. The concentrations of pixels identified as containing iron-bearing carbonate within the greater area of calcite+montmorillonite compares well with this description. If the uranium-bearing sandstones are associated with the fault zones indicated by iron-bearing carbonate, then the distribution of this mineral identified in the imaging spectrometer data indicates a large area stretching from the known mineral occurrence, Khanneshin southern, to the northwest, covering a distance of more than 11 km (figs. 21B–17 and 21B–19) in which additional sampling and study is warranted.

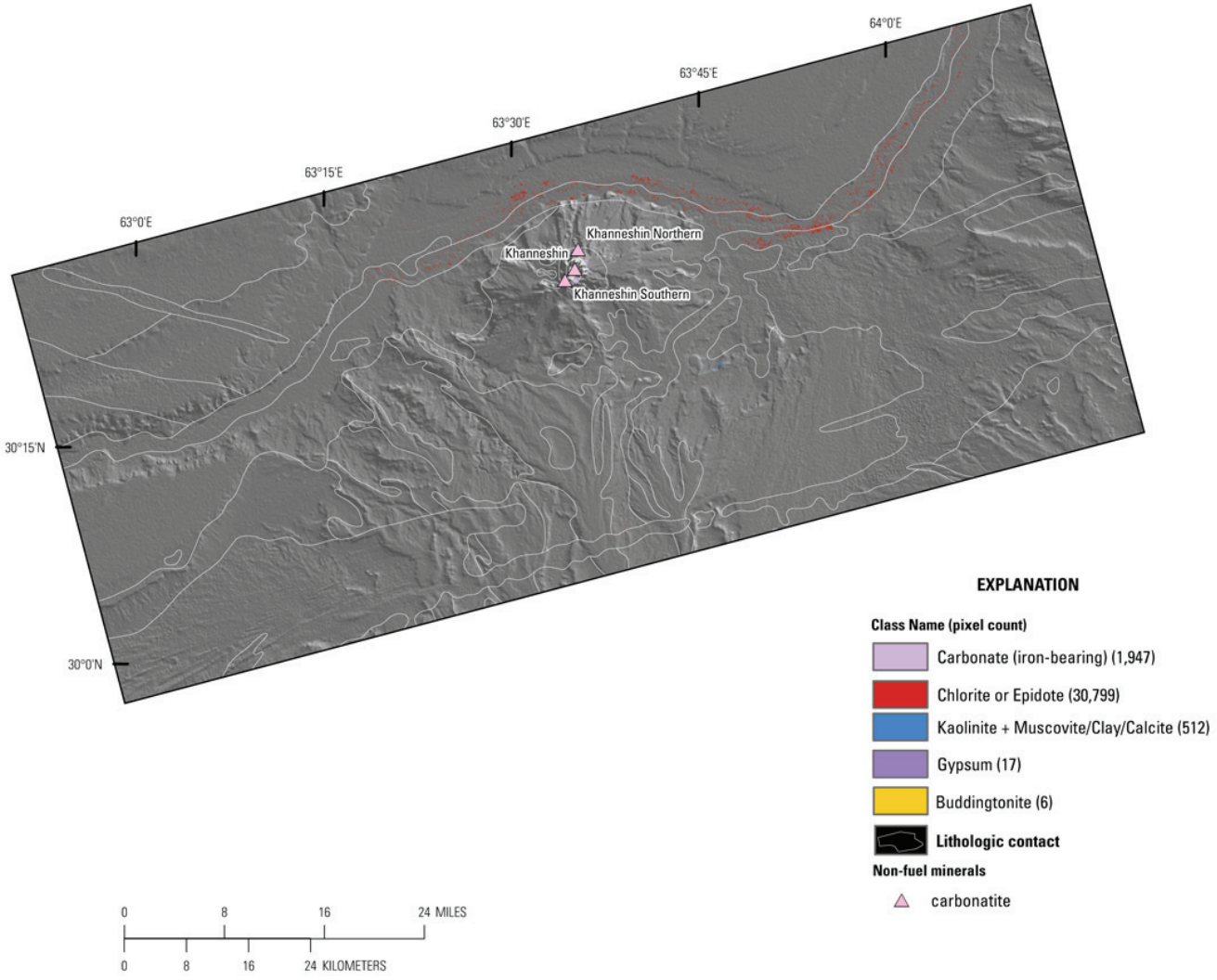

Figure 21B–11. Map of distribution of common alteration minerals derived from HyMap data in the Khanneshin area of interest.

The northern uranium-thorium Khanneshin mineral occurrence is hosted in sandy claystone in a 2,000-m-long and up to 25-m-wide silicified zone (Abdullah and others, 1977). The mineral detections in this vicinity are mainly calcite+montmorillonite in the 2-µm map, with isolated areas of pixels more closely matched to montmorillonite or calcite (fig. 21B–15) and hematite in the 1-µm map (fig. 21B–16). The area north of the Khān Nishīn Ghar volcano that includes the scattered pixels most closely matched to montmorillonite clay within the more widely mapped calcite+montmorillonite class corresponds to the area of host rock described as sandy claystone (red dashed line, fig. 21B–15). The area covers over 700 hectares, including the Khanneshin northern mineral occurrence near the northwest corner.

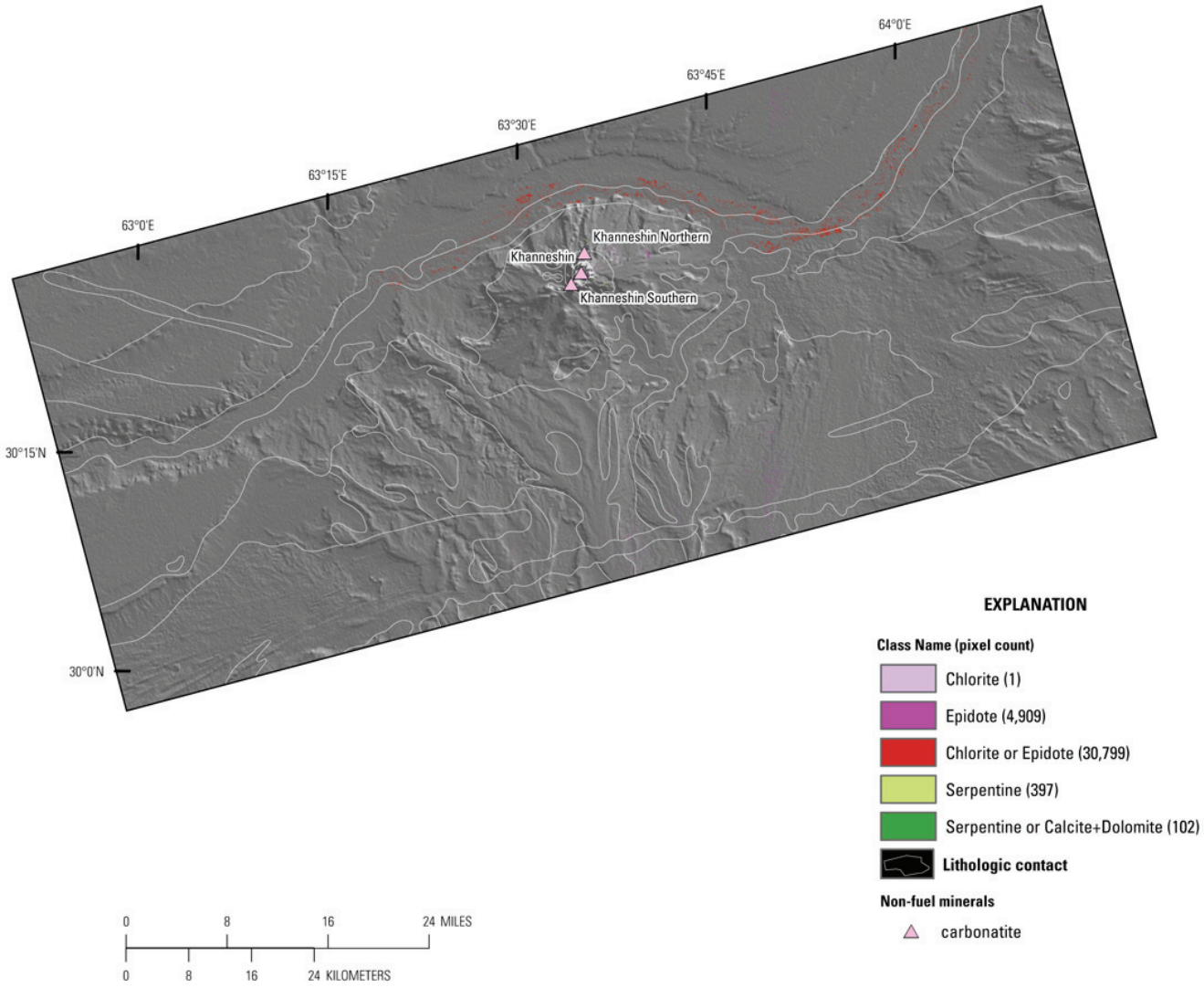

Figure 21B–12. Map of distribution of common secondary minerals derived from HyMap data in the Khanneshin area of interest.

The vent of the Khān Nishīn Ghar volcano, including the Khanneshin mineral occurrence, is composed of ankerite-barite carbonatite associated with an 800-m-long, 50-m-wide fluorite-rich zone that is eroded to a 150-m depth and contains abundant earthy-yellow strontium-barium zones grading from 0.3 to 6.0 percent REE, more than 10 percent strontium, and 10 percent barium. Fluorite in the complex also contains REE, grading 0.6 percent cesium, 0.5 percent lanthanum, and 0.05 percent uranium. The results from the 2-μm analysis of the imaging spectrometer data show carbonatitic rocks in the intrusive body and surrounding area are identified as matching the calcite spectrum in the reference library (fig. 21B–15). The results for the 1-μm analysis in the area indicate the presence of a variety of iron-bearing minerals ranging from hematite and goethite (fig. 21B–18) to various ferric minerals (fig. 21B–16). Together, the mineral maps show the carbonatitic rocks, including the Khanneshin REE occurrence, are defined by calcite in the 2-μm map and the lack of iron-bearing minerals in the 1-μm map. The distribution pattern of pixels with this composition includes the central vent of the volcano and mapped intrusive rocks, as well as a larger area of carbonatitic rocks stretching north and east of the mapped intrusive body (green pixels indicating calcite and calcite+muscovite/illite, fig. 21B–15). The strength and shape of the carbonate absorption feature, centered near 2.3 μm, shows variation throughout the area. These variations may be related to the concentration of REE and uranium in the Khanneshin AOI. In addition, a great deal of mineral variation around the main areas of

carbonatite are expressed (1) in the 2-μm map by occurrences of dolomite, serpentine or calcite+dolomite (fig. 21B–17), montmorillonite (fig. 21B–15), and iron-bearing carbonate (fig. 21B–19), and (2) in the 1-μm map by various types of ferric and ferrous iron absorption features (figs. 21B–16 and 21B–18). In conjunction with the carbonate absorption feature, the variations in iron-absorption may be related to the concentrations of REE and uranium in the Khanneshin AOI.

Further analyses of the imaging spectrometer data are warranted. These studies should include the measurement of field samples of REE-bearing rocks using laboratory spectrometers. By including such measurements in the reference spectral library, the HyMap imaging spectrometer data, collected at ~ 30 m pixel size over the carbonatite area, may be analyzed to directly detect the signatures of rare earth minerals (REMs). The REM absorption features are unique and very strong, and could be detected in cases where they only cover a small portion of a pixel. Higher spatial resolution imaging spectrometer data would have even greater capability to detect REMs if they occur in small zones or patches and/or at low concentrations.

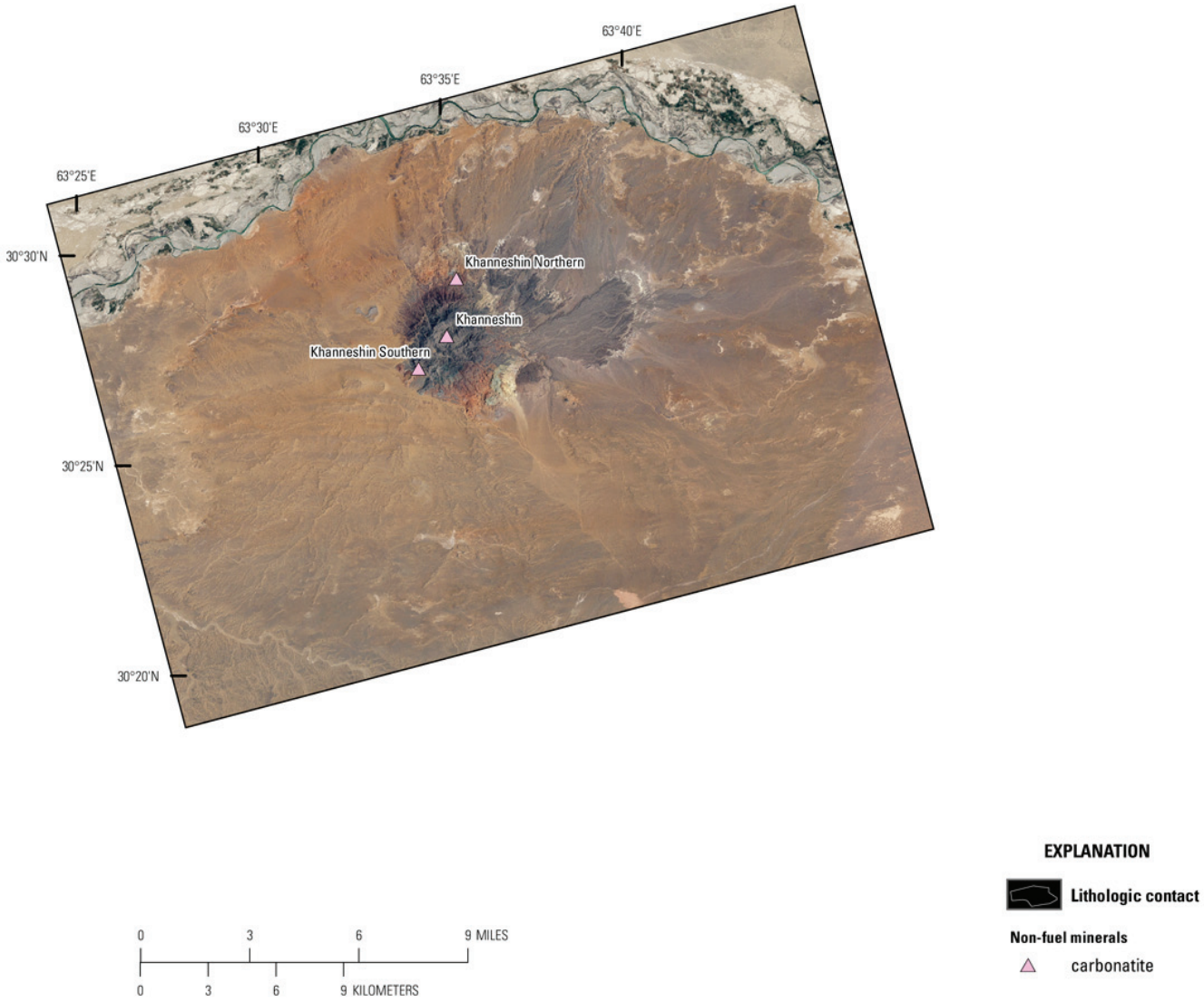

Figure 21B–13. Contrast-enhanced Landsat Thematic Mapper natural color image of the Khanneshin volcano subarea of the Khanneshin area of interest. Sites of known mineralization by deposit type are from Peters and others (2007).

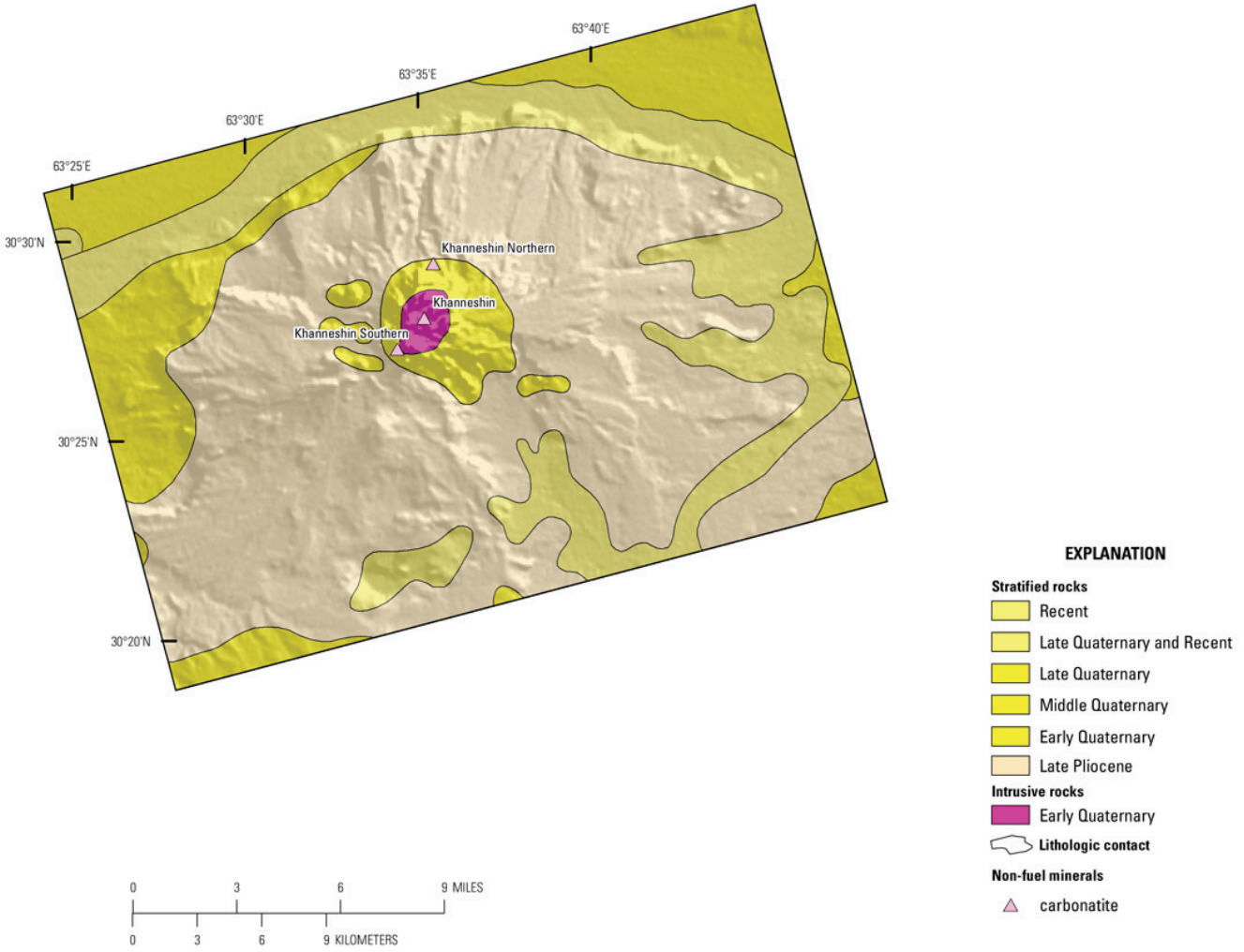

Figure 21B–14. Sites of known mineralization by deposit type (Peters and others, 2007) on the geologic map of the Khanneshin volcano subarea of the Khanneshin area of interest from 1:500,000-scale geologic map of Afghanistan (Doebrich and others, 2006; Abdullah and Chmyriov, 1977).

21B.5 Summary

The illite and muscovite classes covered most of the eastern portion of the Khanneshin AOI. The calcite mixed with clay class was widely distributed throughout the area, but was most concentrated in the northern and western portions of the AOI. Pixels matched to iron-bearing carbonate, calcite, dolomite, and mixtures of dolomite with montmorillonite and/or calcite were concentrated in the mapped intrusive rock unit of the Khān Nishīn Ghar volcano and adjacent areas. Distinct patterns of montmorillonite and kaolinite clays, calcite, and gypsum occurred in clusters scattered throughout the central and eastern portions of the AOI. The Fe^{3+} Type 1 class was distributed in a pattern similar to that of the illite/muscovite classes, also covering the majority of the eastern portion of the Khanneshin AOI. Pixels matching the Fe-hydroxide class were also mapped in contiguous patterns in this part of the AOI, in addition to being present around the mapped unit of volcanic rocks.

Maps of the Khanneshin volcano subarea, containing REE and uranium occurrences, showed carbonatite rocks to be defined by calcite in the 2-µm map and the lack of iron-bearing minerals in the 1-µm map. The distribution pattern of pixels with this composition included the central vent of the Khān Nishīn Ghar volcano and mapped intrusive rocks, as well as a larger area of carbonatitic rocks stretching north and east of the mapped intrusive body. The strength and shape of the carbonate absorption feature in the HyMap imaging spectrometer data showed variation throughout the carbonatite area. These

variations may be related to the concentration of REE and uranium in the Khanneshin AOI. In addition, a great deal of mineral variation around the main areas of carbonatite was detected in the 2-μm map by occurrences of dolomite, calcite+dolomite or serpentine, montmorillonite, and iron-bearing carbonate, and in the 1-μm map by various types of ferric and ferrous-iron absorption features. In conjunction with the carbonate absorption feature, the variations in iron absorption may be related indirectly to the concentrations of REE and uranium in the Khanneshin AOI.

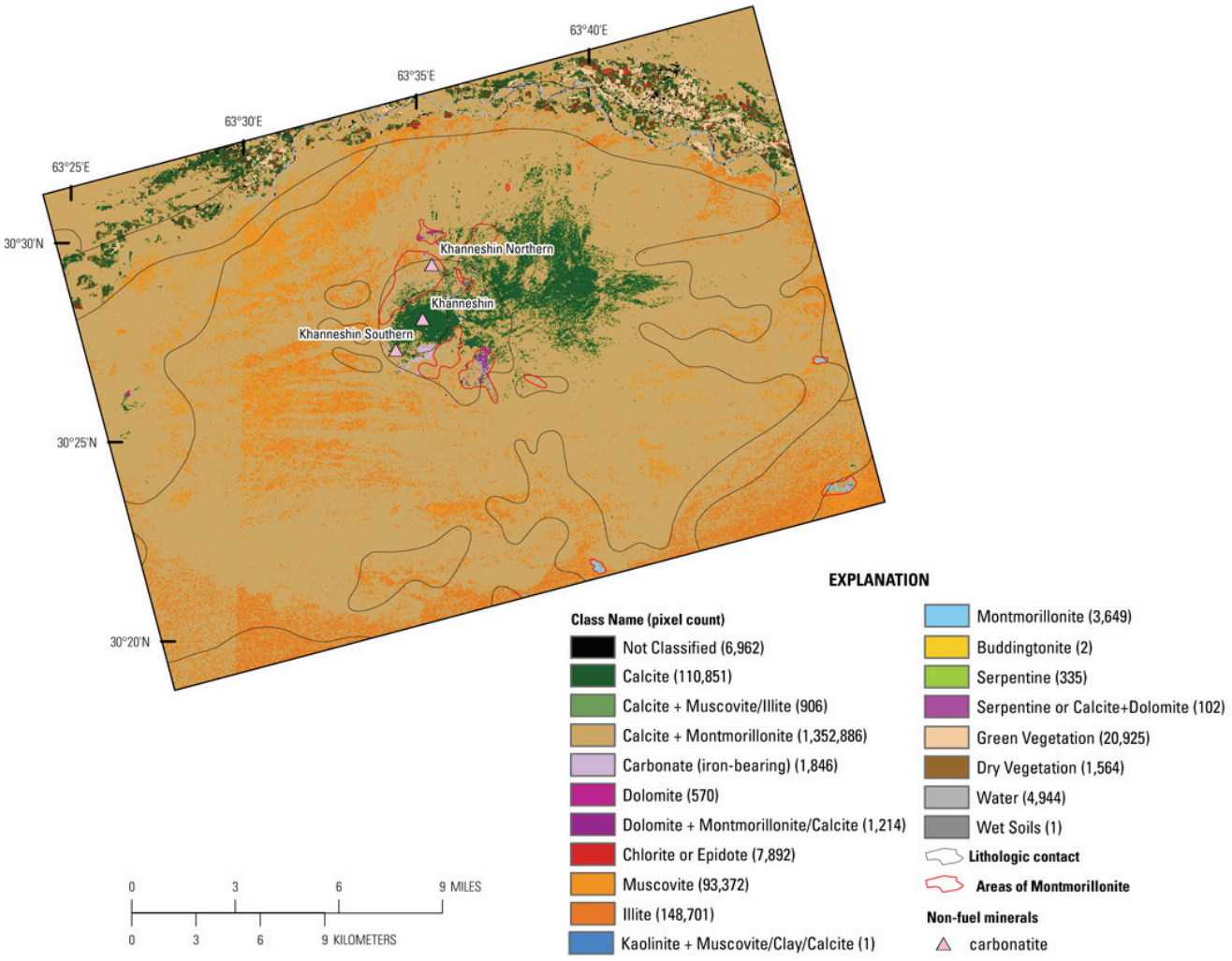

Figure 21B–15. Map of carbonates, phyllosilicates, sulfates, altered minerals, and other materials derived from HyMap data in the Khanneshin volcano subarea of the Khanneshin area of interest. Sites of known mineralization by deposit type are from Peters and others (2007).

Concentrations of pixels identified as containing iron-bearing carbonate within the more widespread calcite+montmorillonite class were found near the southern margin of the Khān Nishīn Ghar volcano in the area around the Khanneshin southern uranium occurrence, matching its description as sandstone intruded by carbonatite dikes along southwest-striking faults, with the fault zones containing ferruginous clay carbonate minerals. If the uranium-bearing sandstones are associated with the fault zones indicated by iron-bearing carbonate, then the imaging spectrometer data indicate a large area with similar composition as the rocks in the vicinity of the known mineral occurrence. This area stretches from the known mineral occurrence, Khanneshin southern, to the northwest, covering a distance of more than 11 km. Additional sampling and study within this area is warranted. The Khanneshin northern uranium-thorium mineral occurrence is hosted in sandy claystone. Around this mineral occurrence, the analysis of imaging spectrometer data revealed a pattern minerals that correspond with the description of

the host rock, defined by scattered pixels with spectra matched to montmorillonite clay within the more widely mapped calcite+montmorillonite class. This pattern was found in the area north of the Khān Nishīn Ghar volcano covering over 700 hectares.

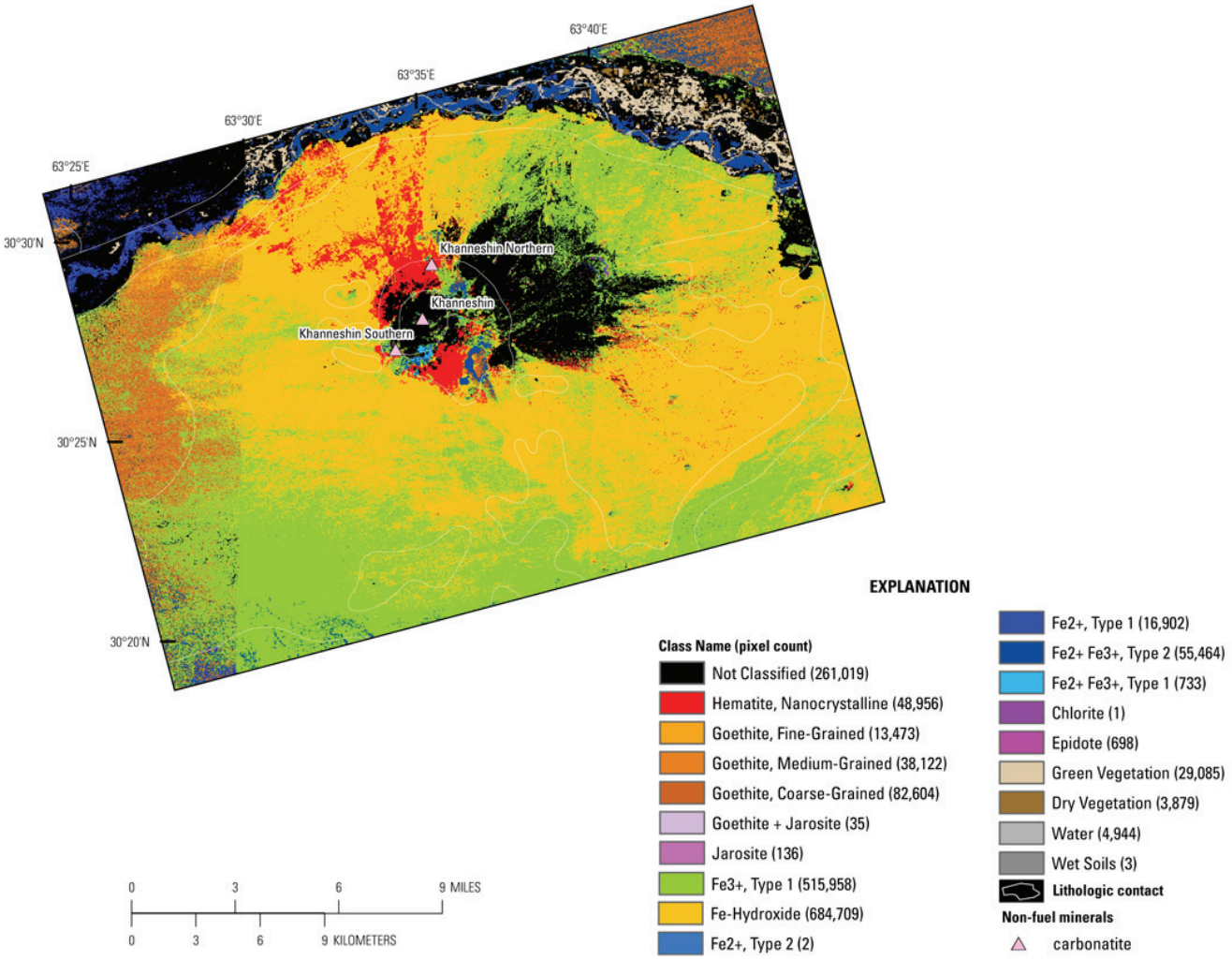

Figure 21B–16. Map of iron-bearing minerals and other materials derived from HyMap data in the Khanneshin volcano subarea of the Khanneshin area of interest. Sites of known mineralization by deposit type are from Peters and others (2007).

Further analyses of the HyMap imaging spectrometer data are warranted. These studies should include the measurement of field samples of REE-bearing rocks using laboratory spectrometers. The HyMap imaging spectrometer data could be analyzed to directly detect the signatures of REM if they occur in great enough abundance within a pixel.

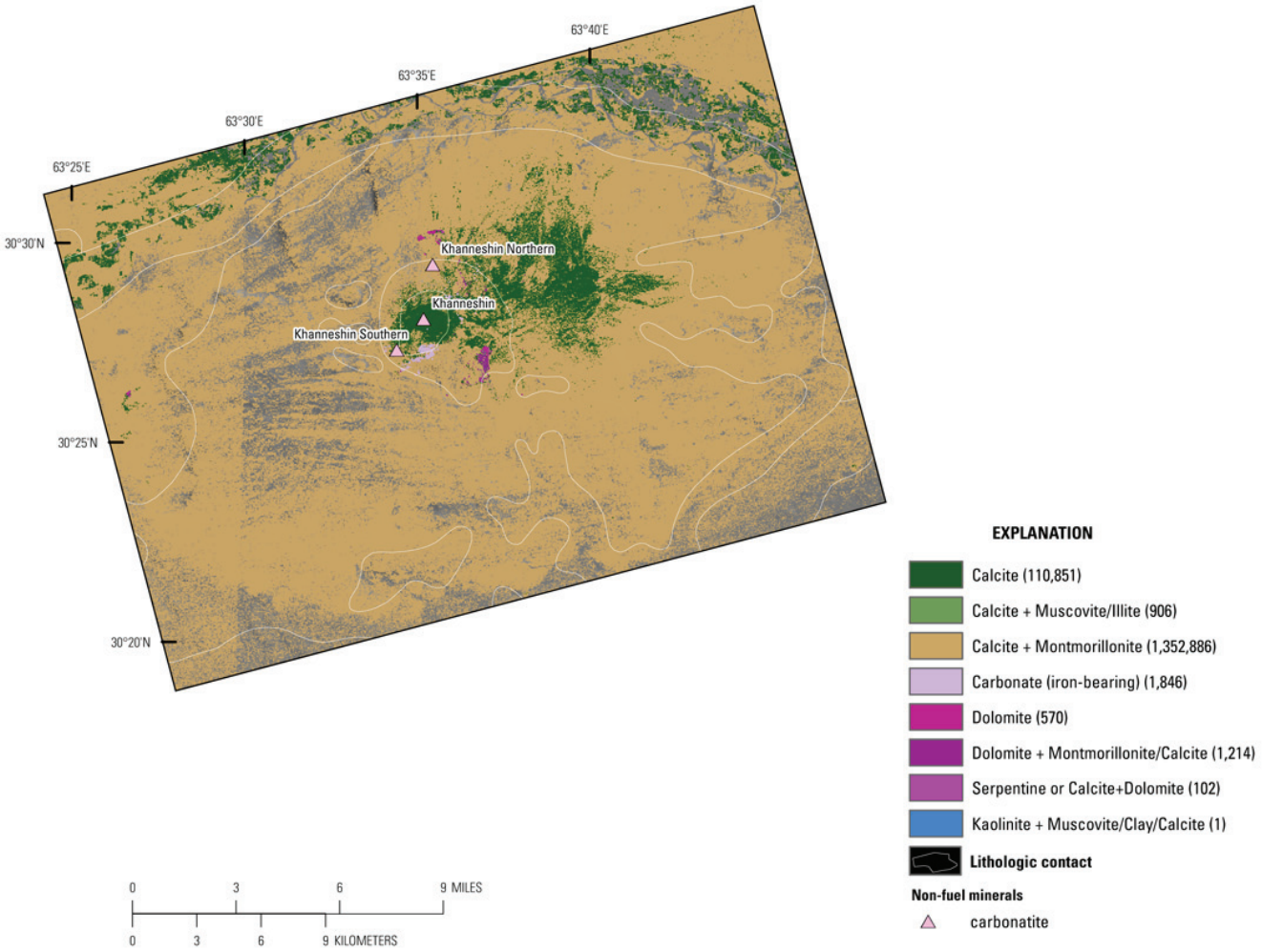

Figure 21B–17. Map of distribution of carbonate minerals derived from HyMap data in the Khanneshin volcano subarea of the Khanneshin area of interest. Sites of known mineralization by deposit type are from Peters and others (2007).

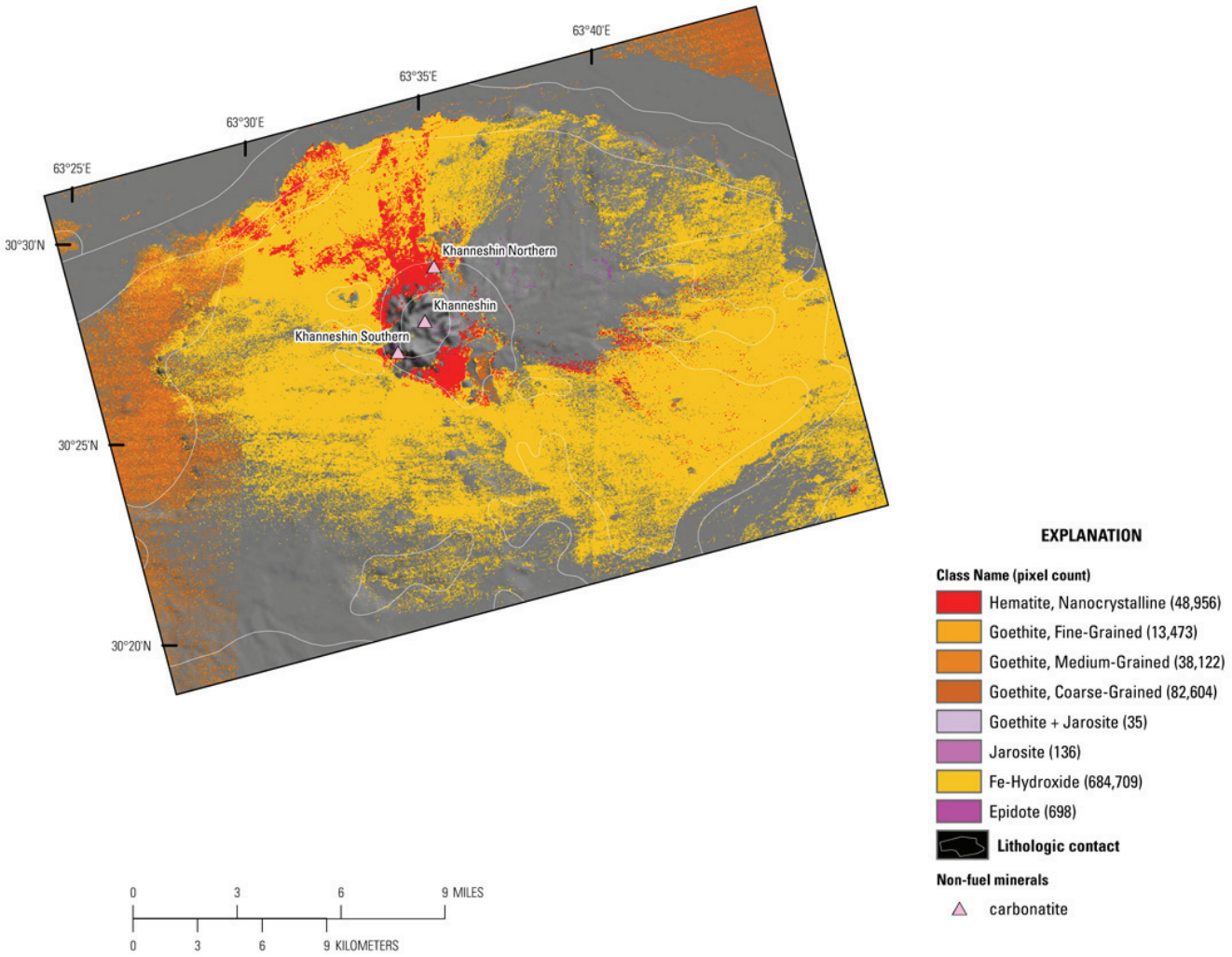

Figure 21B–18. Map of distribution of iron oxide and hydroxide derived from HyMap data in the Khanneshin volcano subarea of the Khanneshin area of interest. Sites of known mineralization by deposit type are from Peters and others (2007).

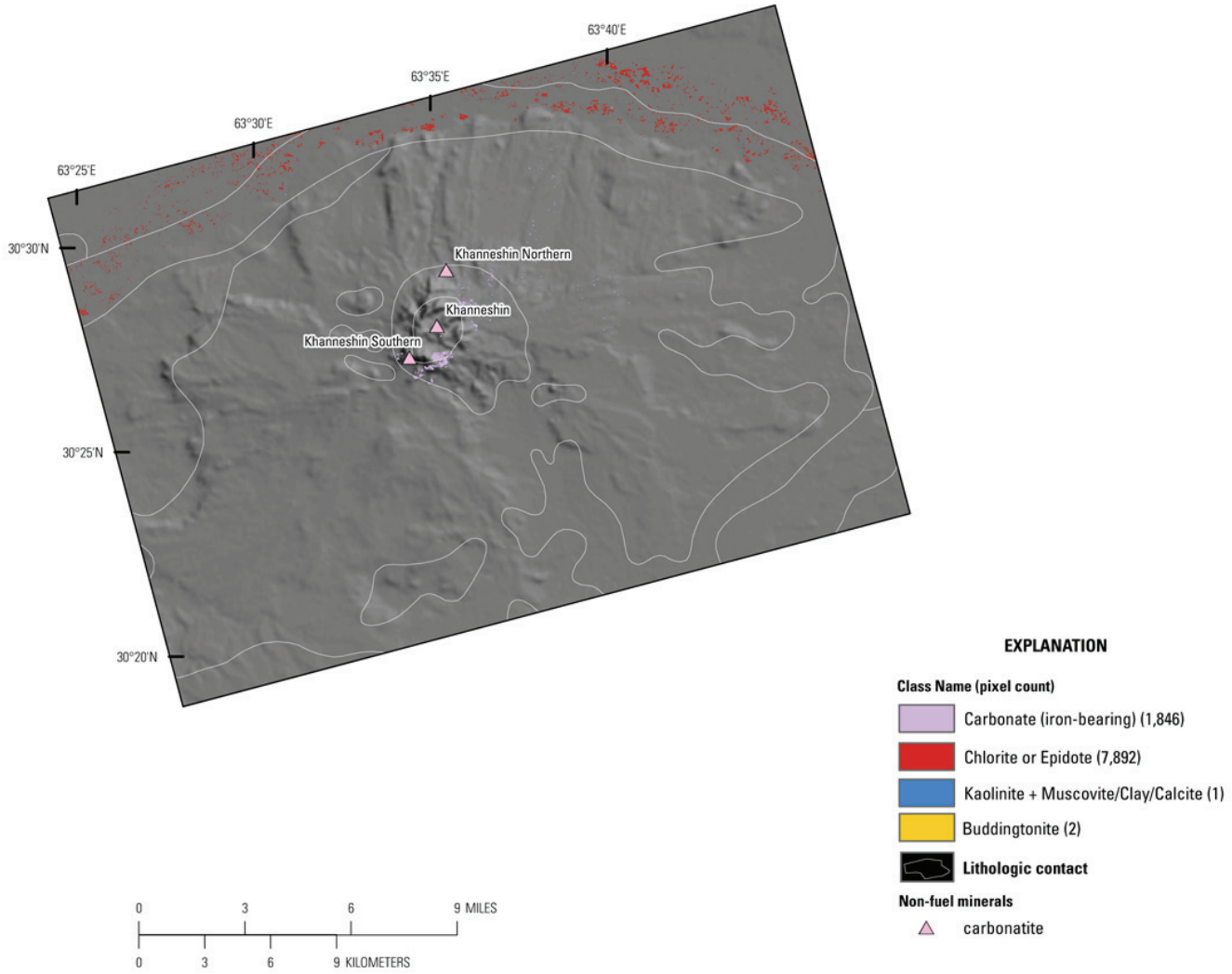

Figure 21B–19. Map of distribution of common alteration minerals derived from HyMap data in the Khanneshin volcano subarea of the Khanneshin area of interest. Sites of known mineralization by deposit type are from Peters and others (2007).

21B.6 References Cited

Abdullah, J., Bordet, P., Carbonnel, J.P., and Pias, J., 1975, Sur l'existence d'un dome recent de carbonatites dans le Registan (Afghanistan du Sud) [The existence of a Recent carbonatite dome in Registan, southern Afghanistan]: Comptes Rendus Hebdomadaires des Seances de l'Academie des Sciences, SerieD: Sciences Naturelles, v. 281, no. 23, p. 1801–1804.

Abdullah, Sh., and Chmyriov, V.M., 1977, Geological map of Afghanistan: Kabul, Afghanistan, Ministry of Mining and Industry of Democratic Republic of Afghanistan, scale 1:500,000.

Abdullah, Sh., Chmyriov, V.M., Stazhilo-Alekseev, K.F., Dronov, V.I., Gannan, P.J., Rossovskiy, L.N., Kafarskiy, A.Kh., and Malyarov, E.P., 1977, Mineral resources of Afghanistan (2d ed.): Kabul, Afghanistan, Republic of Afghanistan Geological and Mineral Survey, 419 p.

Alkhazov, V.Yu., Atakishiyev, Z.M., and Azimi, N.A., 1977, Geologiya i poleznyye iskopayemyye rannechetvertichnogo karbonatitovogo vulkana Khanneshin (Yuzhnyy Afghanistan) [Geology and mineral resources of an early Quaternary carbonatite volcano in Khanneshin, South Afghanistan]: Sovetskaya Geologiya, no. 4, p. 131–136.

Alkhazov, V.Yu., Atakishiyev, Z.M., and Azimi, N.A., 1978, Geology and mineral resources of the early Quaternary Khanneshin carbonatite volcano (Southern Afghanistan): International Geology Review, v. 20, no. 3, p. 281–285.

Cocks, T., Jenssen, R., Stewart, A., Wilson, I., and Shields, T., 1998, The HyMap airborne hyperspectral sensor—The system, calibration and performance, *in* Schaepman, M., Schlapfer, D., and Itten, K.I., eds., Proceedings of the 1st EARSeL Workshop on Imaging Spectroscopy, 6–8 October 1998, Zurich: Paris, European Association of Remote Sensing Laboratories, p. 37–43.

Davis, P.A., 2007, Landsat ETM+ false-color image mosaics of Afghanistan: U.S. Geological Survey Open-File Report 2007–1029, 22 p. (Also available at *http://pubs.usgs.gov/of/2007/1029/*.)

Doebrich, J.L., and Wahl, R.R., comps., *with contributions by* Doebrich, J.L., Wahl, R.R., Ludington, S.D., Chirico, P.G., Wandrey, C.J., Bohannon, R.G., Orris, G.J., Bliss, J.D., and ____, 2006, Geologic and mineral resource map of Afghanistan: U.S. Geological Survey Open File Report 2006–1038, scale 1:850,000, available at *http://pubs.usgs.gov/of/2006/1038/*.

Hoefen, T.M., Kokaly, R.F., and King, T.V.V., 2010, Calibration of HyMap data covering the country of Afghanistan, *in* Proceedings of the 15th Australasian Remote Sensing and Photogrammetry Conference, Alice Springs, Australia, September 12–17, 2010, p. 409, available at *http://dl.dropbox.com/u/81114/15ARSPC-Proceedings.zip/*.

King, T.V.V., Kokaly, R.F., Hoefen, T.M., and Knepper, D.H., 2010, Resource Mapping in Afghanistan Using HyMap Data, *in* Proceedings of the 15th Australasian Remote Sensing and Photogrammetry Conference, Alice Springs, Australia, September 12–17, 2010, p. 500.

King, T.V.V., Kokaly, R.F., Hoefen, T.M., Dudek, K. and Livo, K.E., 2011, Surface materials map of Afghanistan—Iron-bearing minerals and other materials: U.S. Geological Survey Scientific Investigations Map 3152–B.

Kokaly, Ray, 2011, PRISM—Processing routines in IDL for spectroscopic measurements: U.S. Geological Survey Open-File Report 2011–1155, available at *http://pubs.usgs.gov/of/2011/1155/*.

Kokaly, R.F., King, T.V.V., and Livo, K.E., 2008, Airborne hyperspectral survey of Afghanistan 2007—Flight line planning and HyMap data collection: U.S. Geological Survey Open-File Report 2008–1235, 14 p.

Kokaly, R.F., King, T.V.V., Hoefen, T.M., Dudek, K. and Livo, K.E., 2011, Surface materials map of Afghanistan—Carbonates, phyllosilicates, sulfates, altered minerals, and other materials: U.S. Geological Survey Scientific Investigations Map 3152–A.

Peters, S.G., Ludington, S.D., Orris, G.J., Sutphin, D.M., Bliss, J.D., and Rytuba, J.J., eds., and the U.S. Geological Survey-Afghanistan Ministry of Mines Joint Mineral Resource Assessment Team, 2007, Preliminary non-fuel mineral resource assessment of Afghanistan: U.S. Geological Survey Open-File Report 2007–1214, 810 p., 1 CD–ROM. (Also available at *http://pubs.usgs.gov/of/2007/1214/*.)

Vikhter, B.Y., Yeremenko, G.K., and Chmyrev, V.M., 1975, Molodoi vulakanogennyi karbonatitovyi kompleks v Afganistane [A young volcanogenic carbonatite complex in Afghanistan]: Sovetskaya Geologiya [Soviet Geology], no. 10, p. 107–116.

Vikhter, B.Y., Yeremenko, G.K., and Chmyrev, V.M., 1976, A young volcanogenic carbonatite complex in Afghanistan: International Geology Review, v. 18, no. 11, p. 1305–1312.

Vikhter, B.Y., Yeremenko, G.K., Chmyrev, V.M., and Abdulla, D., 1978, Pliocene-Quaternary volcanism of Afghanistan: International Geology Review, v. 20, no. 5, p. 525–536.